coatings

MDPI

Review

TiO_2-Based Photocatalytic Coatings on Glass Substrates for Environmental Applications

Shuang Tian [1], Yuxiao Feng [1], Ziye Zheng [1] and Zuoli He [1,2,*]

[1] Shandong Key Laboratory of Water Pollution Control and Resource Reuse, Shandong Key Laboratory of Environmental Processes and Health, School of Environmental Science and Engineering, Shandong University, Qingdao 266237, China
[2] Weihai Research Institute of Industrial Technology of Shandong University, Shandong University, Weihai 264209, China
* Correspondence: zlhe@sdu.edu.cn

Abstract: To address environmental pollution and energy shortage issues, titanium dioxide (TiO_2)-based photocatalysts, as an efficient pollution removal and fuel production technology, have been widely used in the field of photocatalysis. In practical applications, TiO_2-based photocatalysts are usually prepared on various substrates to realize the separation of the catalyst from water and improve photocatalytic stability. Herein, the research progress of TiO_2-based heterogeneous photocatalytic coatings deposited on glass substrates with various deposition techniques is reviewed. Such TiO_2-based composite coatings obtained using different techniques showed excellent self-cleaning, pollution removal, air purification, and antibiosis performance. The various deposition techniques used for the preparation of TiO_2 coatings, such as wet chemical deposition (WCD), electrodeposition, physical vapor deposition (PVD), and chemical vapor deposition (CVD) were discussed together with photocatalytic applications by highlighting the typical literature. Finally, the challenges and prospects of developing TiO_2-based heterogeneous coatings were put forward.

Keywords: TiO_2; coatings; glass substrates; deposition; photocatalysis

check for updates

Citation: Tian, S.; Feng, Y.; Zheng, Z.; He, Z. TiO_2-Based Photocatalytic Coatings on Glass Substrates for Environmental Applications. *Coatings* **2023**, *13*, 1472. https://doi.org/10.3390/coatings13081472

Academic Editor: Michael Nolan

Received: 18 July 2023
Revised: 11 August 2023
Accepted: 14 August 2023
Published: 21 August 2023

Copyright: © 2023 by the authors. Licensee MDPI, Basel, Switzerland. This article is an open access article distributed under the terms and conditions of the Creative Commons Attribution (CC BY) license (https://creativecommons.org/licenses/by/4.0/).

1. Introduction

Environmental pollution and energy shortage have been persistent problems faced by researchers committed to finding solutions [1–3]. Semiconductor-based photocatalysis is a green and sustainable advanced oxidation process (AOP) that can directly convert green solar energy into chemical energy [4–6]. Therefore, semiconductor photocatalysis has been widely used in the environmental and energy fields [7–13]. Various semiconductor materials have been developed as photocatalysts, such as TiO_2, g-C_3N_4, ZnO, Bi-based, and Ag-based materials [14–23]. As shown in Figure 1, TiO_2 was the most researched photocatalyst among many semiconductor photocatalysts due to its good photostability, low cost, and environmental friendliness [24–27]. However, the low photocatalytic efficiency of TiO_2 under visible light limits its practical applications due to the low absorption of visible light and high rate of photogenerated carrier recombination [28–30]. Metal and non-metal loading or doping and heterojunction building could enlarge the light response range and improve charge separation to address these issues [31–37]. In addition, nanostructured TiO_2-based composites are difficult to separate and recover in a flow system or aqueous suspension, resulting in low efficiency and stability during environmental applications [38–41]. It is worth noting that TiO_2 nanoparticles (NPs) will inevitably remain in the environment and migrate in water and soil, which poses a risk to human and environmental health [42,43]. Photocatalytic coatings could realize the immobilization of nanosized photocatalysts and have emerged as an efficient strategy for solving these problems [44]. The obtained photocatalytic coating system eliminates the steps of filtering and recovering

the catalyst after use, which allows the coating to be directly reused and run continuously for a long time without a large amount of catalyst loss and inactivation [45–47].

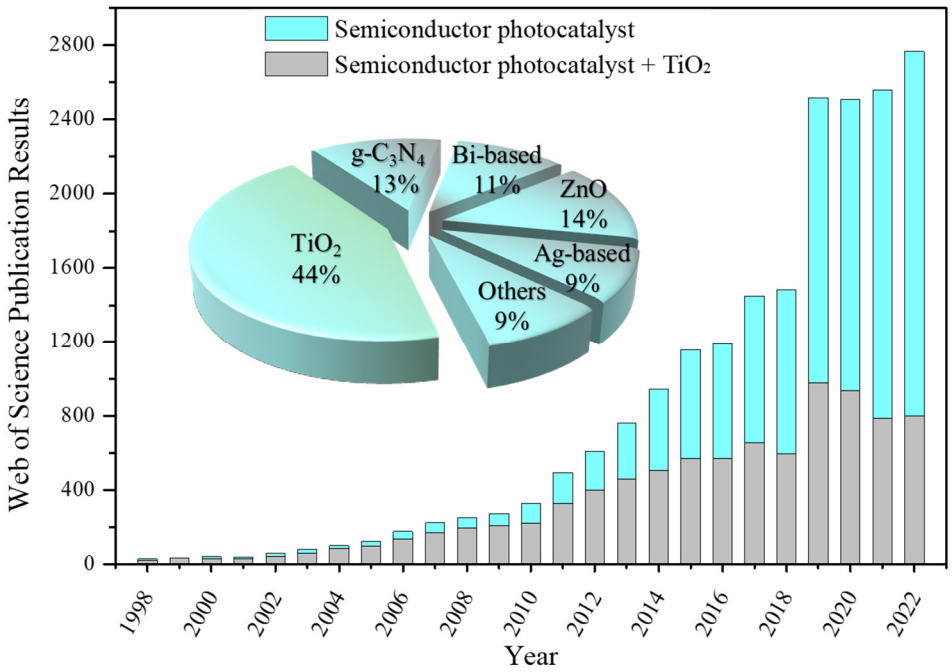


Figure 1. Publication trends in semiconductor photocatalysis technology. Bar graph represents Web of Science data analysis results for yearly publications from 1998 to 2022, using keywords "semiconductor photocatalyst; semiconductor photocatalyst + TiO_2", and the inset pie chart indicates the proportion of TiO_2, g-C_3N_4, Bi-based, ZnO, Ag-based, and other semiconductor photocatalysts used in semiconductor photocatalysis technology between 1998 and 2022, respectively.

Photocatalytic coatings have been applied from the laboratory to the industrial fields in our daily life [48–51]. Researchers have deposited TiO_2 nanocomposites onto various substrates to explore their photocatalytic performance [52]. Due to its high-temperature resistance and chemically inert properties, glass has shown great potential in depositing TiO_2-based photocatalytic heterogeneous coatings as a substrate using various techniques [53–55]. Although some studies have comprehensively summarized TiO_2-based photocatalytic coatings, including their preparation methods and applications [56], it is necessary to summarize and discuss the deposition strategies of TiO_2-based photocatalytic coatings on glass substrates with different photocatalytic applications. Thus, we intend to provide a review of TiO_2-based photocatalytic heterogeneous coating deposition technology on glass substrates and their corresponding applications in the environmental field.

2. The Basic Principle of TiO_2 Photocatalysis

It was observed by Fujishima and Honda [57] in 1972 that using a TiO_2 electrode in an electrochemical cell under UV irradiation led to water splitting even when no external voltage was applied, indicating the photocatalytic activity of TiO_2 and thus opening up a new field of applications. TiO_2 has become one of the most promising materials in the field of photocatalysis [58]. In the photocatalytic process, there are three main crystal phases of TiO_2: rutile, anatase, and brookite [59]. In all these three forms, Ti atoms are coordinated to O atoms, forming TiO_6^{2-} octahedral units. The formation of cells for the three TiO_2 phases depends on how the TiO_6^{2-} octahedral units contact the neighboring octahedrons. It is shown in Figure 2 that adjacent octahedra units in anatase, rutile, and brookite share four, two, and three edges, respectively [59]. All of these crystalline structures could act as photocatalysts. The effect of the crystal phase on the photocatalytic performance of TiO_2

has attracted extensive attention. At present, pure- and mixed-phase TiO_2 photocatalysts have been synthesized and applied in photocatalysis.

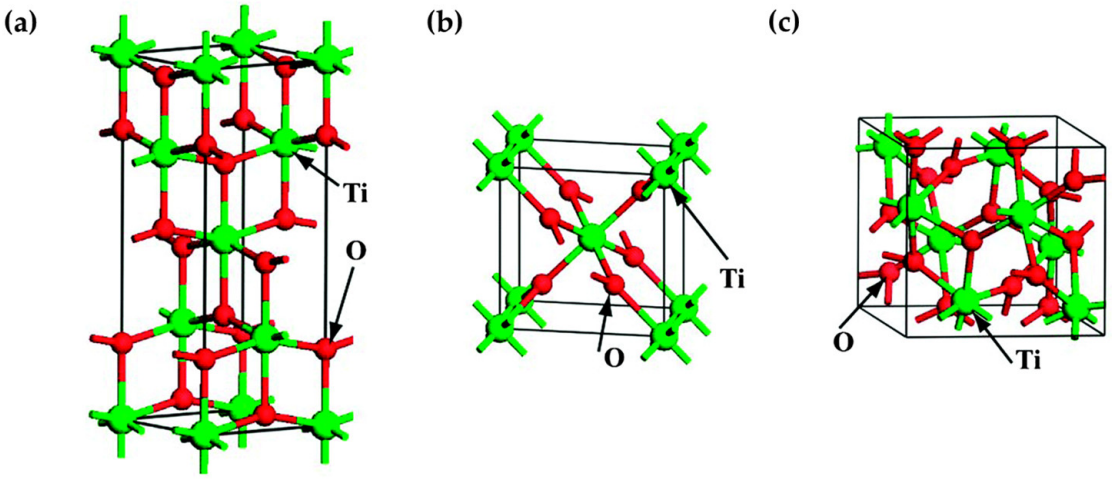


Figure 2. Schematic diagram of regular cells for anatase (**a**), rutile (**b**), and brookite (**c**). Reproduced with permission from [59]. Copyright 2014, Royal Society of Chemistry.

The photocatalytic process for TiO_2 involving the formation of advanced oxidants is illustrated in Figure 3. Bandgaps (E_g) of the rutile and anatase phases are about 3.0 and 3.2 eV, respectively [60]. When the light ($hv \geq E_g$) irradiates on TiO_2, its photon absorption causes electrons to be excited from the valence band (VB) to the corresponding conduction band (CB), resulting in photogenerated electrons (e^-) and positively charged holes (h^+). Photogenerated e^- and h^+ are reducing agents and solid oxidants, respectively. When they migrate to the surface of TiO_2, they will undergo redox reactions with the adsorbed oxygen or water molecules to form superoxide anion radicals ($O_2^{\bullet -}$) and hydroxyl radicals (•OH), respectively. Other reactive oxygen species, such as hydroperoxide radical (•OOH) and H_2O_2, can also be formed by further redox processes, dimerization, or disproportionation during the photocatalytic process [61,62].

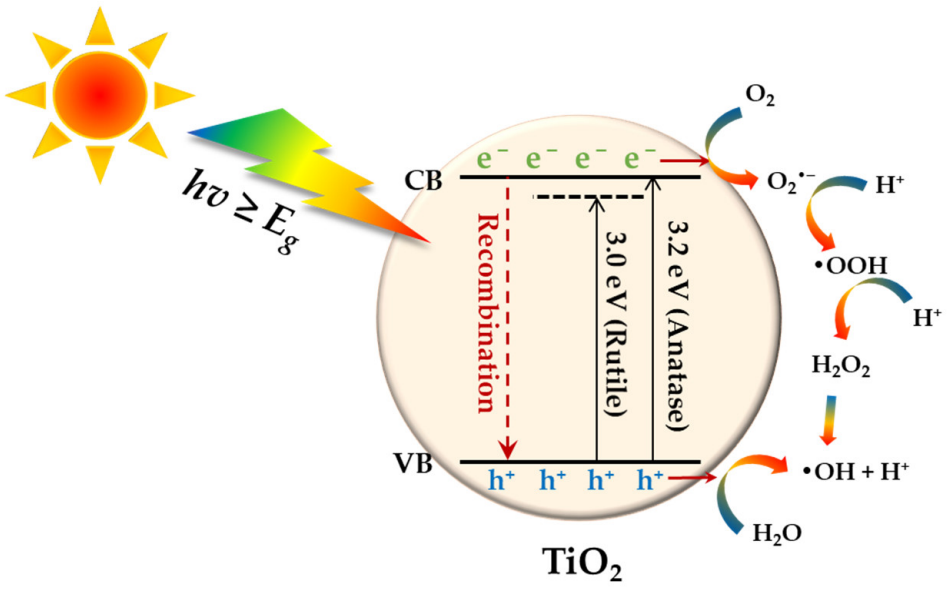


Figure 3. Schematic diagram of TiO_2 photocatalytic mechanism.

3. Preparations and Applications of TiO_2-Based Photocatalytic Coatings

The selection of the substrate is an essential step in photocatalytic coatings. The substrate materials should have good properties, such as good adhesion, high-temperature stability and strong adsorption of pollutants of TiO_2 coatings. Previous studies have shown that common substrates for fixing heterogeneous photocatalysts based on TiO_2 nanostructures include glass [38,63], steel [64], metal or metal oxide [65], polymers [54,66], ceramics [67], cement mortar [68], zeolite [69], non-woven fabric [70], and latex [71], etc. Although there are many options for choosing a substrate for photocatalytic coatings, glass substrates are preferred for photocatalytic research. Glass is low-cost, easily fabricated, highly chemically/physically/thermally stable, and optically attractive, which makes it an ideal material for photocatalytic coatings [72]. Glass substrates have the desirable property of light transparency, which guarantees better photocatalytic performance [73]. The photocatalytic activities of photocatalytic glass-based coatings are determined by fixing methods. The standard deposition methods for depositing TiO_2 nanostructured heterogeneous photocatalytic coatings onto glass materials as substrates are given in the following chapters, such as wet chemical deposition methods (dip coating, spin coating, spray coating), electrodeposition, physical vapor deposition (including magnetron sputtering and pulsed laser deposition), and chemical vapor deposition and other techniques.

3.1. Wet Chemical Deposition

3.1.1. Dip Coating

The dip-coating method is a low-cost and easy-to-operate process that is one of the most commonly employed techniques for depositing TiO_2 nanoparticles (NPs) on glass materials [74]. The dip-coating method involves growing a thin film on the glass substrate by immersing it in a precursor solution containing the photocatalytic material to be deposited. The sol-gel method is often used to prepare TiO_2 precursor solutions in a typical dip-coating process [75]. In addition, before depositing the photocatalytic coating, it is necessary to clean the selected glass material with plasma or wash it with a specific solution, such as acids [76], organic solvents, or neutral detergents [77]. After the precursor solution and glass substrate are prepared, the dip-coating process is started (as shown in Figure 4). The glass substrate is immersed in the pre-solution for a period of time by means of dip coating equipment, and then the substrate is extracted at a certain speed. The immersion time and dipping times can determine the coatings' thickness. After the deposition, the obtained films are dried and annealed to promote the crystallization of TiO_2. It should be emphasized that two or more precursor solutions may be used in the preparation of TiO_2-based heterogeneous photocatalytic coatings.

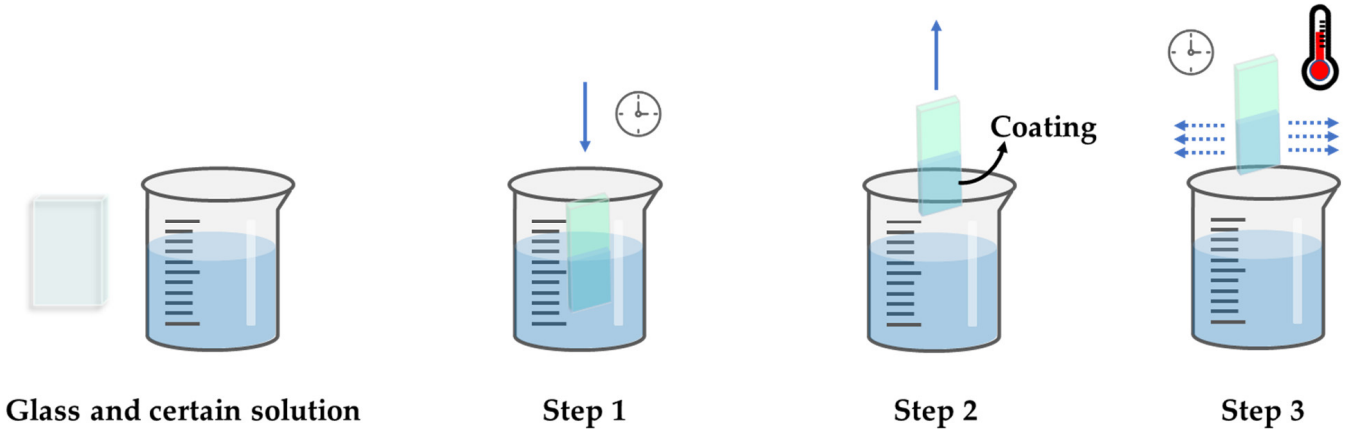


Figure 4. Schematic diagram of the steps in the dip-coating process.

According to the literature [78], the amount and crystalline phases of TiO_2 can significantly affect the photocatalytic performances of the obtained coatings. The increase in dip-coating times only increases the thickness of the coating, but dose not change the crystal phase. The crystalline phases are determined by the annealing temperatures in the post-thermal process. Moreover, glass materials often contain many sodium ions. If the photocatalytic coating is too thin, the sodium diffusion from the glass substrate could adversely affect the photocatalytic activity. Overall, when using dip-coating technology to obtain photocatalytic coating, we should carefully control the number of dip-coating cycles and proper annealing procedures. Appropriate parameters will produce the desired TiO_2 coating with suitable coating thickness and crystal phase. Rajendran et al. [79] deposited activated carbon-doped TiO_2 heterogeneous film onto a glass substrate with titanium tetraisopropoxide as the starting material using a sol-gel-assisted dip-coating technique. The coatings were dried at 200 °C for 30 min and then annealed at 400 °C or 600 °C for 1 h. The coating crystal structures obtained were anatase and rutile, respectively. When annealed at 600 °C, the crystal structure changed from the anatase type to the rutile type. The intensity of XRD patterns increased with film thickness and annealing temperature. In addition, the authors found that the doping of activated carbon affected the photocatalytic performance of TiO_2 coatings. Similarly, Rapsomanikis et al. [80] synthesized Ce-TiO_2 coatings via the sol-gel method and deposited them on the borosilicate glass using dip coating. The coatings were dried at room temperature for 1 h and calcined at 500 °C at a heating rate of 5 °C/min. The introduction of Ce effectively expanded the response range to visible light and reduced the recombination rate of e^-/h^+, thus enhancing the photocatalytic decolorization of Basic Blue 41 (BB-41) in visible light.

Moreover, Manna et al. [77] reported a TiO_2-ZrO_2 photocatalytic heterogeneous coating with efficient photocatalytic removal of methylene blue (MB) dye from water. TiO_2-ZrO_2 composite photocatalysts were fabricated using a sol-gel process using zirconium (IV) oxychloride octahydrate powder (ZOC), titanium (IV) isopropoxide (TTIP), and block co-polymer (surfactant). Subsequently, TiO_2-ZrO_2 was dip-coated on the float glass substrate. Then, the coatings were thermally treated at 400 °C with a 1.5 °C/min heating rate after drying at 80 °C. After successfully introducing ZrO_2, the composite film exhibited a spherical and clumped distribution morphology, as shown in Figure 5a,b. The TiO_2-ZrO_2 composite coating also had a regular texture and extremely root-mean-square (RMS) roughness surface, thus exhibiting superhydrophobicity and self-cleaning. As shown in Figure 5c, in the presence of TiO_2-ZrO_2 coating, the characteristic peak intensity of MB was significantly reduced after 20 min of ultraviolet irradiation. The obtained mesoporous TiO_2-ZrO_2-coated float glass had a self-cleaning capability, photocatalytic performance, and antireflective properties (Figure 5d), which could effectively replace the empty texture solar cover glass in the market. However, the performances of the TiO_2-ZrO_2-coated float glass on a large scale need to be evaluated in actual applications. Additionally, Bagheri et al. [81] synthesized an optimized CNT-modified TiO_2/WO_3/CdS ternary nanocomposite and deposited it on fluorine-doped tin oxide (FTO) glass using the sol-gel and dip-coating methods. As shown in Figure 5e, CNT-modified TiO_2/WO_3/CdS particles aggregated on the FTO glass surface and formed a photocatalytic coating with a thickness of about 781.50 nm. TiO_2 was composited with CdS (2.25 eV), WO_3 as a light-storing material, and CNTs with a large electron storage capacity in this heterojunction. Consequently, heterojunction formation significantly reduced electronic bandgap value and increased visible light absorption. The CNT/TiO_2/WO_3/CdS coatings on FTO glass could be used as a photoanode in the photocatalytic fuel cell to degrade Reactive blue 19 (RB19) (Figure 5g). In the optimal light intensity (890 lm), 99.9% and 70% removal efficiency for RB19 and COD were obtained, respectively (Figure 5f).

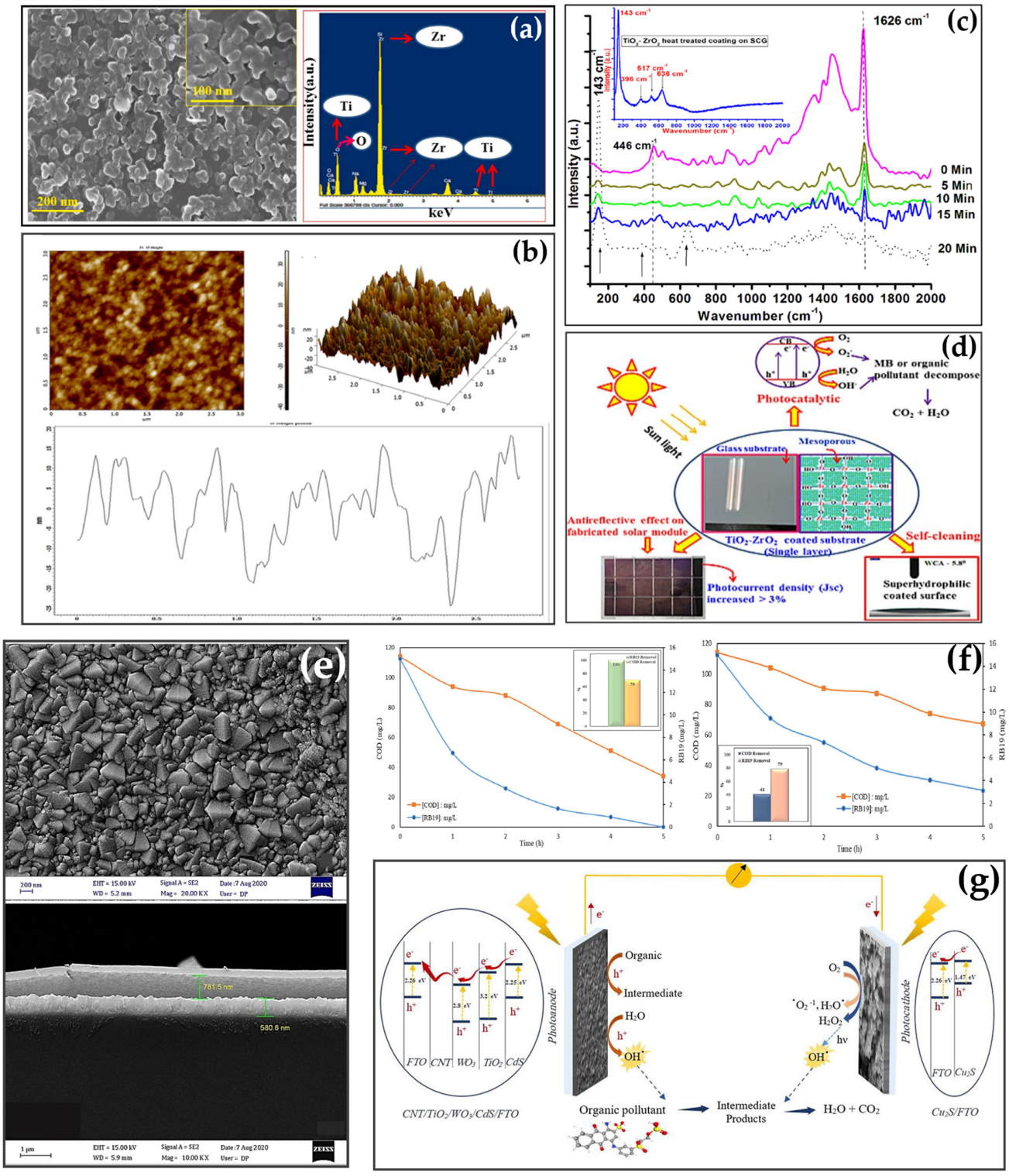


Figure 5. (**a**) FESEM images and EDX pattern of the coating; (**b**) 2D- and 3D-AFM images of the mesoporous TiO_2-ZrO_2 coating with surface roughness curve; (**c**) the decomposition of MB on the TiO_2-ZrO_2 coating under UV exposure by Raman spectra; (**d**) three properties of TiO_2-ZrO_2 coating, reproduced with permission from [77]. Copyright 2023, Elsevier Ltd.; (**e**) FESEM images of the top view and side view of the CNT/TiO_2/WO_3/CdS coatings; (**f**) the time-dependent RB19 and COD removal curves during the photoelectrochemical process under the light intensities of 13 lm (up) and 890 lm (down); (**g**) the mechanism of the photocatalytic fuel cell with CNT/TiO_2/WO_3/CdS/CNT photoanode, reproduced with permission from [81]. Copyright 2022, Elsevier B.V.

3.1.2. Spin Coating

Spin coating technology is an advanced, cheap, easy-to-control uniform coating deposition technology that can be used to deposit NPs onto different substrate surfaces [82,83]. A typical spin-coating process is present in Figure 6, and the process can be divided into three stages after preparing the material and substrate. Firstly, the substrate is placed onto the cage of the spin coater, and the prepared solution is dropped onto the upper surface of the glass substrate. Then, a wet film is produced by centrifugal force during rotation. As the spinning proceeds, the excess liquid flows away from the substrate. Finally, solvent evaporation leads to the coating's formation. Further calcination may be required to crystallize the deposited coatings for the desired application. The spinning speed and spin-coating recycling times can determine the coatings' thickness. Thus, the thickness of the coating can be controlled.

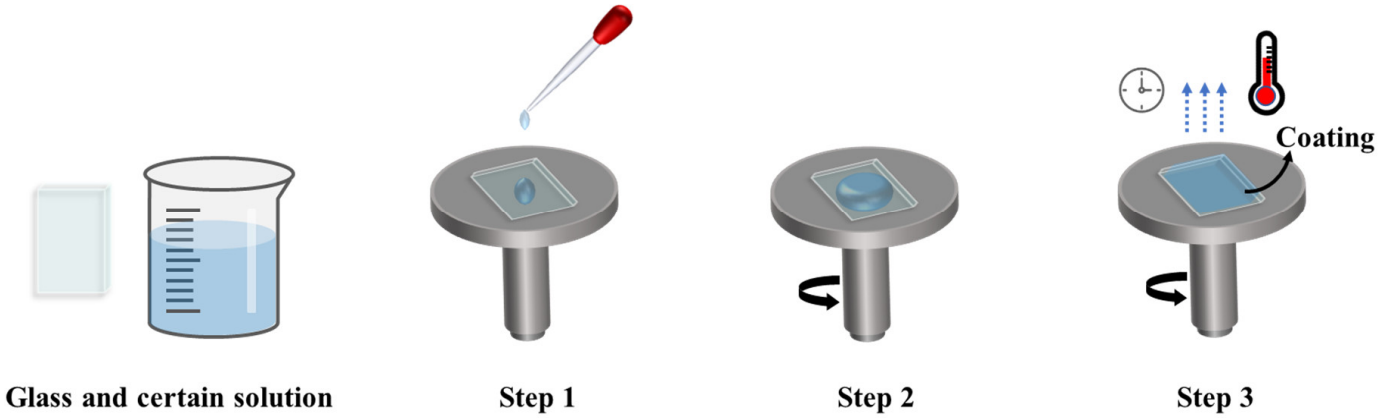


Figure 6. Schematic diagram of the steps in the spin-coating process.

Peeters et al. [84] reported a self-cleaning borosilicate coating; a TiO_2 film embedded with gold (Au) NPs was deposited on a glass surface by spin coating (Figure 7a). After being calcined at 550 °C for 3 h with a 1 °C/min heating rate, uniform, smooth, highly transparent, and photoactive Au NPs with anatase TiO_2 thin coatings were obtained. Au NPs with an average diameter of 16 ± 4 nm distributed on TiO_2 coatings at different depths (Figure 7b,c). Compared with commercial Pilkington Activ^{TM}, embedding Au NPs leads to better photocatalytic self-cleaning activity under dark and irradiation conditions (Figure 7d). The plasmonic effect of Au NPs was fully utilized to alleviate the problem of poor visible light response of TiO_2 coating. Therefore, the self-cleaning glass with Au-TiO_2 composite coatings has great application potential under actual sunlight. Further study is needed to verify the self-cleaning application of the developed photocatalytic coatings in real life. Komaraiah et al. [85] covered a glass substrate with high-quality nanocrystalline Fe-doped TiO_2 using a simple spin-coating technique, producing a coating for MB decomposition under the irradiation of visible light. Compared with pure TiO_2, the bandgap decreased with the increase in Fe concentration, and the 7% Fe-doped TiO_2 (FTO7) film exhibited a high decolorization rate (96.7%) for MB with excellent stability in 10 cycles (see Figure 7e–g). The mechanism of the FTO7 coating is shown in Figure 7h. Incorporating Fe^{3+} into the TiO_2 lattice substituted Ti^{4+}, resulting in a charge imbalance. Then, Fe^{3+} trapped the photogenerated electron and hole to form Fe^{2+} and Fe^{4+}, respectively. The formation of Fe^{2+} and Fe^{4+} decreased the distance between CB and VB, which can enhance the charge carrier separation. As a result, the doping of appropriate Fe^{3+} ions was beneficial to the improvement of photocatalytic activity.

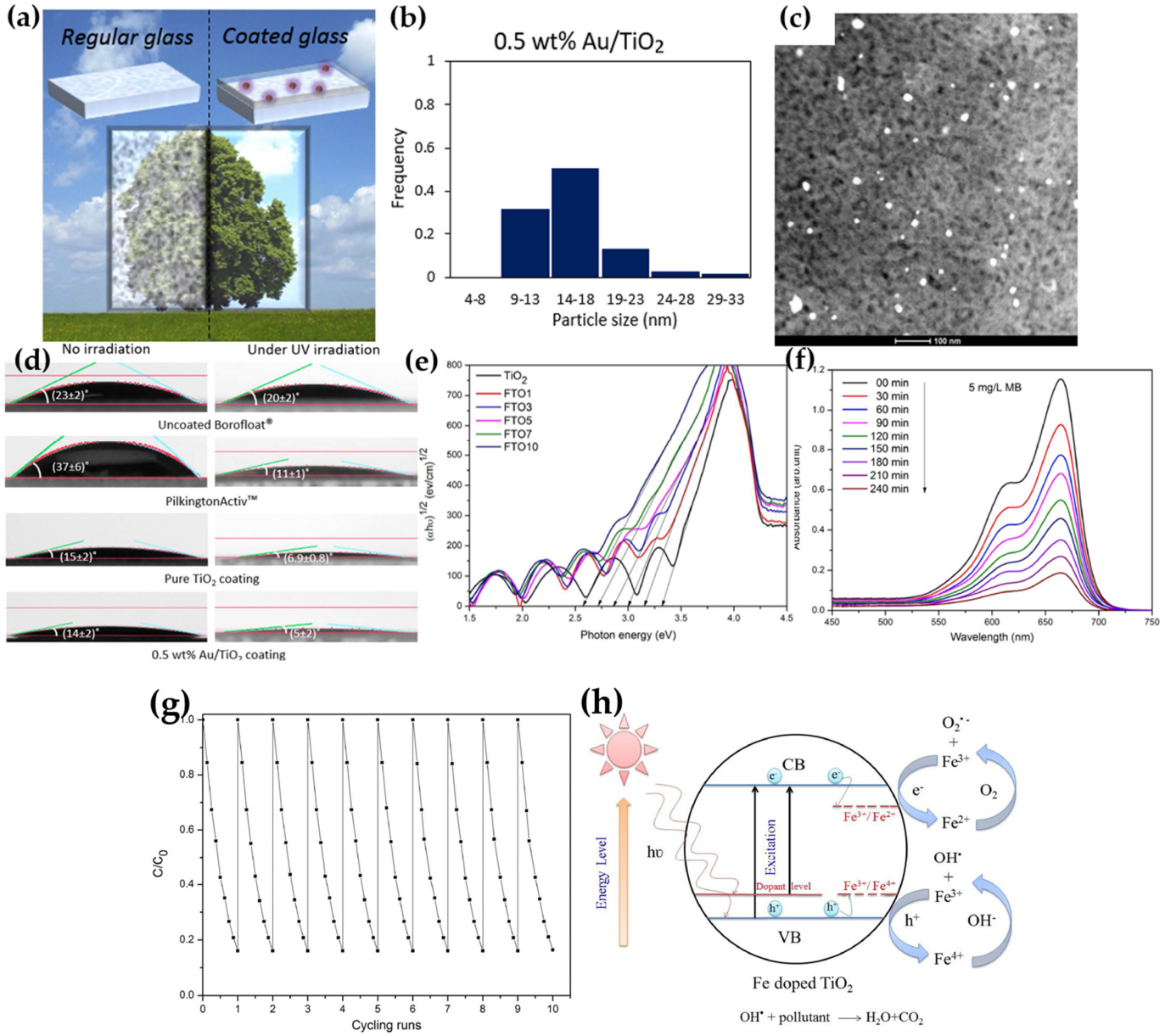


Figure 7. (**a**) Self-cleaning effect diagram of regular glass and coated glass; (**b**) the particle size distribution of Au NPs in the 0.5 wt% Au/TiO_2; (**c**) TEM image of 0.5 wt% Au/TiO_2; (**d**) images of the contact angle of a droplet of 4 µL water on different clean samples, reproduced with permission from [84]. Copyright 2020, Elsevier B.V.; (**e**) the $(\alpha hv)^{1/2}$ change of Fe-doped TiO_2 thin films with photon energy; (**f**) UV-Vis absorption spectra of MB solution with FTO7 coating; (**g**) cycling operation in the MB photodegradation with the presence of FTO7 coating under irradiation of visible light; (**h**) schematic diagram of the mechanism of Fe-doped TiO_2 coatings, reproduced with permission from [85]. Copyright 2019, Elsevier B.V.

Romero-Morán et al. [86] deposited TiO_2 NPs on soda-lime glasses using a water-diluted spin-on-glass (SOG) solution to fabricate TiO_2/SiO_2 composite coatings using the spin-coating method (Figure 8a). The TiO_2/SiO_2 coatings prepared with TiO_2 NPs suspensions with different crystalline phases showed significant differences in surface roughness, antibacterial activity, and the generation of •OH (Figure 8b–d). The antibacterial activity was consistent with the trend of •OH production by photocatalysis: Degussa (P25)-TiO_2/SiO_2 > anatase-TiO_2/SiO_2 > rutile-TiO_2/SiO_2. In addition, pNDA photo-bleaching experiments in the presence of scavengers were conducted to further study the embedding

of amorphous SiO_2 and the embedded TiO_2 NP suspensions with three crystalline phases during photocatalysis. The relationship between the generation of •OH and the charge carriers transfer mechanism of different TiO_2/SiO_2 composite coatings was also mainly explained in Figure 8d. Hernández-Del Castillo et al. [87] compared TiO_2 and In-Ni co-doped TiO_2 (T-InNi) coatings on glass substrates using the spin-coating method. TiO_2 and T-InNi coatings had high roughness and porous texture, with an average thickness of 3.59 and 3.37 µm, respectively (Figure 9a). The co-doping of In and Ni caused oxygen vacancy defects in the composite films, significantly inhibiting the recombination of e^-/h^+ pairs and boosting light absorption from the narrowed bandgap (Figure 9b,c). The obtained coatings were conducted to remove eosin yellow (EY) from drinking water, as shown in Figure 9d–f. The T-InNi coatings exhibited a 97.5% degradation rate after 5 h by UV irradiation treatment and a 75% under natural solar light, which was higher than that of TiO_2 coatings. The detailed photocatalytic mechanism of T-InNi coatings is present in Figure 9g. When exposed to UV and solar light, T-InNi with reduced bandgap was more easily excited to produce e^- and h^+. The e^- and h^+ reacted with oxygen dissolved in water and water to form $O_2^{\bullet -}$ and •OH, which can be used to degrade EY.

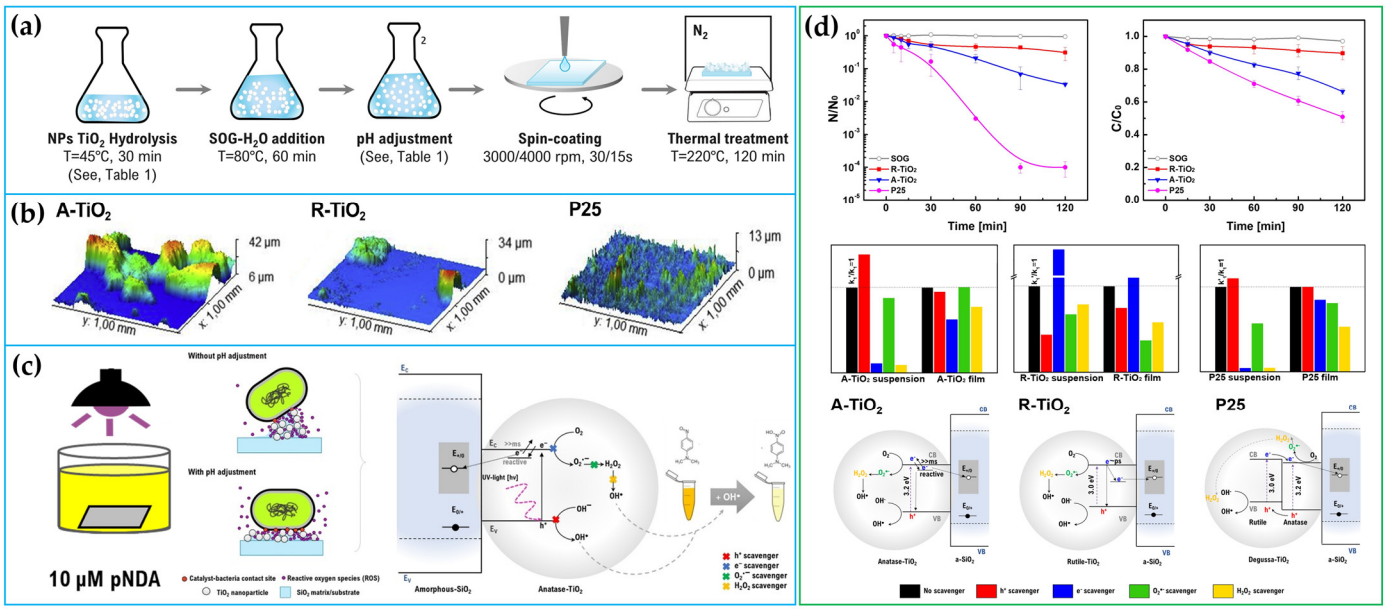


Figure 8. (**a**) Scheme of the preparation process of TiO_2/SiO_2 composite coatings; (**b**) 3D non-contact optical profilometer images of TiO_2/SiO_2 coatings; (**c**) evaluation of antimicrobial activity and •OH generation; (**d**) curves of *E. coli* survival rates and pNDA photobleaching versus irradiation time using samples without pH adjustment and analysis of pNDA photobleaching kinetic rate constants with and without scavengers, reproduced with permission from [86]. Copyright 2020, Elsevier B.V.

3.1.3. Spray Coating

Compared with dip coating and spin coating, the coating obtained by the spraying process is rougher, which can obtain a larger surface area and improve its photocatalytic activity [88,89]. The classic spray-coating technique is efficient for obtaining high-purity coatings due to its relatively low cost and simple equipment [89,90]. After preparing a certain suspension and pretreating the substrate, the suspension was sprayed on the glass substrate from a nozzle, and the coating obtained on the glass is dried and calcined at a controlled time and temperature (Figure 10).

Zong et al. [91] deposited fluorosilicone/SiO_2-TiO_2 (FSi/SiO_2-TiO_2) on a glass substrate by spray coating. The obtained coatings had obvious self-cleaning performance and photocatalytic activity, which effectively prevents many natural pollutants from depositing on the outdoor coated glasses due to ultraviolet radiation. However, fluorosilane

used for surface modification to obtain low surface energy is expensive and may damage the environment. Therefore, using environmentally friendly chemicals to produce superhydrophobic surfaces would be desirable. For example, Wang et al. [92] deposited PDMS-modified SiO_2-TiO_2 ternary composite onto the surface of a glass surface using spray coating to obtain a SiO_2-TiO_2@PDMS coating with excellent self-cleaning performance and photocatalytic activity. Compared with fluorosilane, PDMS is a cost-effective material with many advantages in environmental protection and safety. The SiO_2-TiO_2@PDMS coating was subjected to a thermal treatment at different temperatures for 2 h. The coatings' wettability and adhesion to water droplets can be adjusted by changing the temperature of thermal treatment. The water contact angles of the SiO_2-TiO_2@PDMS coating with a "lotus effect"-like self-cleaning capability after heat treatment at 25 °C and 400 °C were 147.8° and 152.2°, respectively (Figure 11a,b). This suggested that high-temperature treatment enhanced the coating hydrophobicity. Excitingly, the outstanding hydrophobicity of the SiO_2-TiO_2@PDMS coating still had a specific degradation performance on methyl orange compared to the blank sample (Figure 11c). In addition, it was found that the coating exhibited liquid repellency under acid (pH = 2), alkaline (pH = 11), and organic dye droplets, which proved the excellent mechanical stability of the coating even when the surface was mechanically scraped and exposed to ultraviolet light, as shown in Figure 11d.

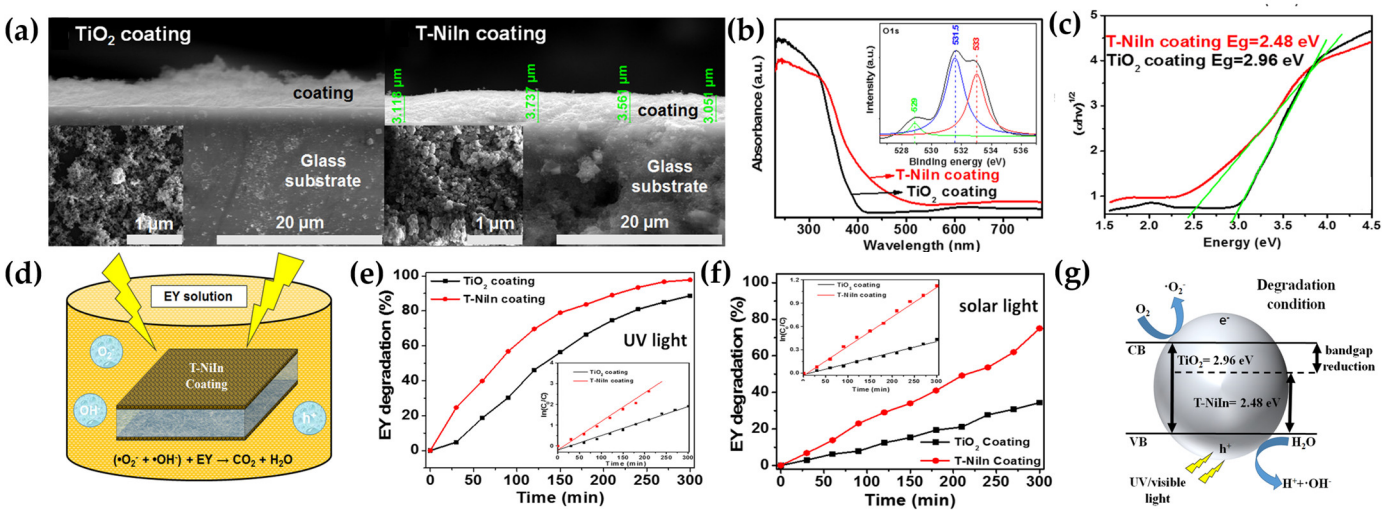


Figure 9. (**a**) SEM images of the cross-section of TiO_2 coating (**left**) and TiO_2-In-Ni coating (**right**); Inset in (**a**) is the top view of the coatings; (**b**) absorbance curves of TiO_2 and TiO_2-In-Ni (illustration of the XPS spectra of the O 1s of the TiO_2-In-Ni coating); (**c**) the $(\alpha hv)^{1/2}$ change of the TiO_2 and TiO_2-In-Ni coatings with energy; (**d**) schematic diagram of the reaction of TiO_2-In-Ni coating; photocatalytic degradation of EY under (**e**) UV light and (**f**) solar light irradiation; (**g**) schematic diagram of the possible photocatalytic mechanism of TiO_2-In-Ni, reproduced with permission from [87]. Copyright 2022, Springer Nature.

For excellent hydrophobic coatings, the durability of the surface properties is critical for practical applications. When coatings are damaged by mechanical wear and/or tear, their superhydrophobic properties will be reduced or even lost. Therefore, epoxy resin (EP) has been progressively used to prepare composite coatings because of its good adhesion and corrosion resistance [93]. Li et al. reported a hydrophobically modified TiO_2 with fluorine-containing hydrogen-containing polysiloxane (F-PMHS) [94]. They prepared an M-TiO_2@EP superhydrophobic composite coating on the glass substrate using EP as the adhesion, which achieved a static contact angle of over 153° for water droplets in a wide pH range (Figure 11e,f). Moreover, the coating had a specific self-cleaning capability and strong hydrophobicities in a simple simulation experiment and in 15-day outdoor experiments (Figure 11f,g). Therefore, these excellent properties allow M-TiO_2@EP coating to be a candidate for promising outdoor and harsh conditions applications. Un-

like the previous preparation steps, the composite coating was prepared by one-step spraying. The preparation method was simple, which makes the coating applicable in large-scale applications.

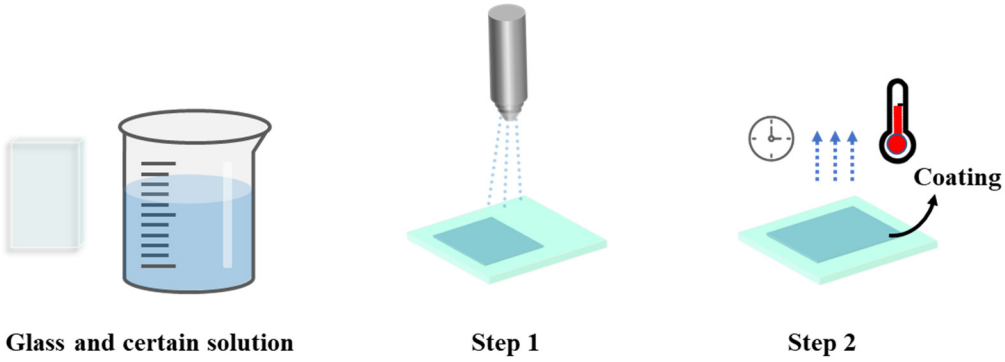


Figure 10. Schematic diagram of the steps in the classical spray-coating process.

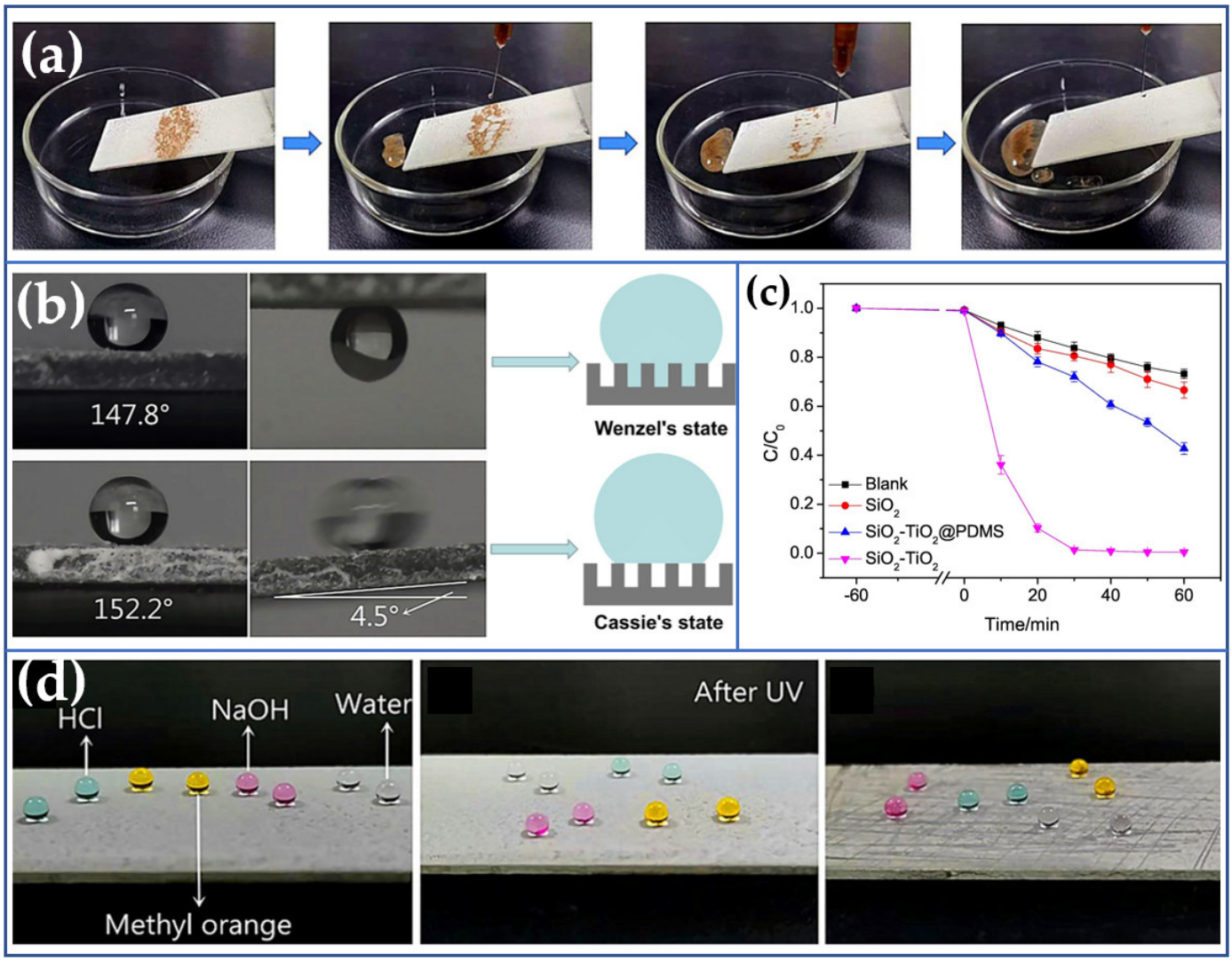


Figure 11. *Cont.*

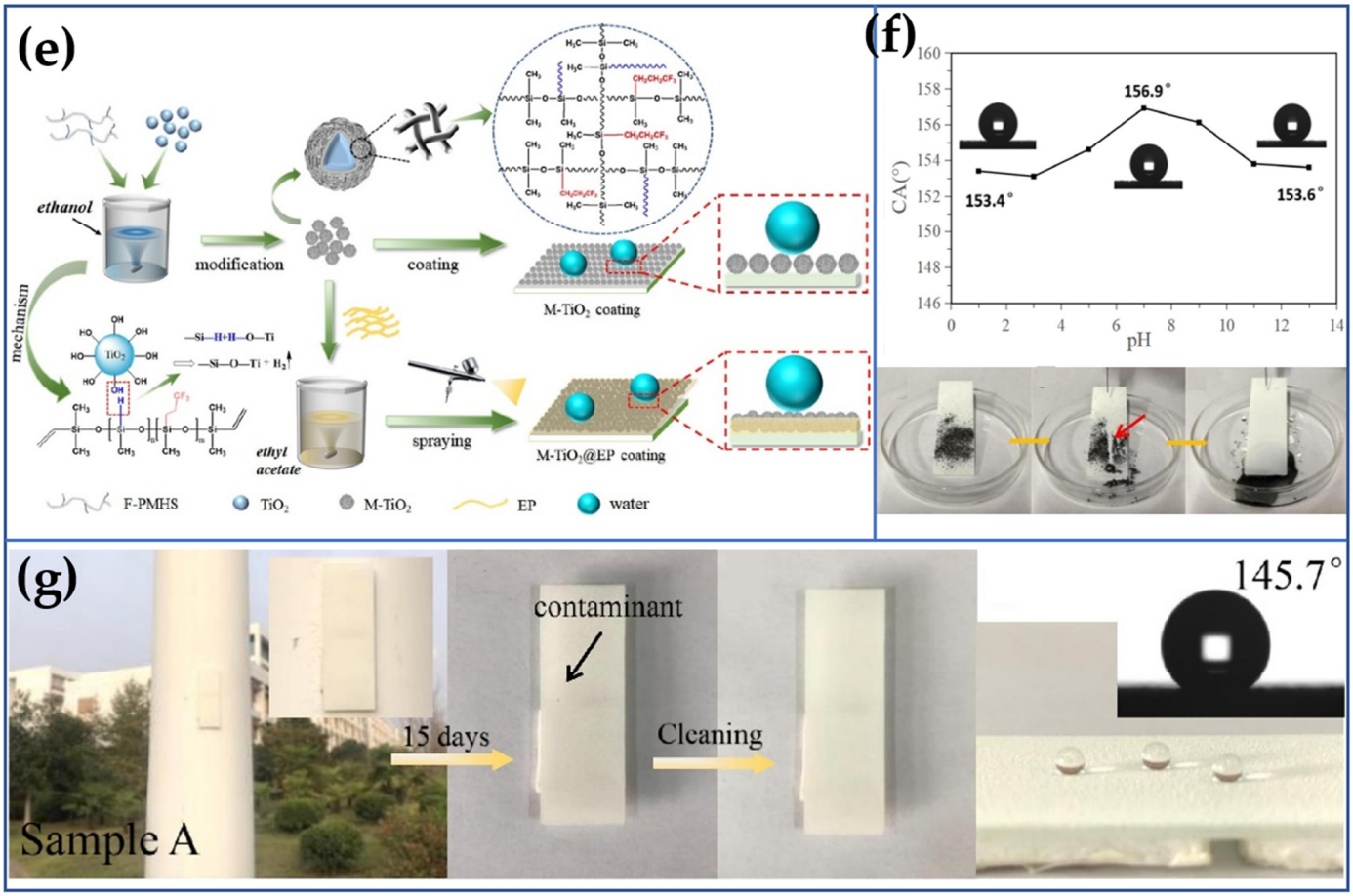


Figure 11. (**a**) Water droplets rolling off to remove dust from the surface of the SiO_2-TiO_2@PDMS coating; (**b**) wettability and adhesion of SiO_2-TiO_2@PDMS-25 (**up**) and SiO_2-TiO_2@PDMS-400 (**down**) coatings to water droplets and the wetting states of water droplets on their surfaces; (**c**) photocatalytic degradation of methyl orange with different samples; (**d**) wettability of water, NaOH solution (stained with rhodamine B), HCl solution (stained with methylene blue), and methyl orange solution on the surface of the SiO_2-TiO_2@PDMS-400 coating, the UV-irradiated and mechanically destroyed SiO_2-TiO_2@PDMS-400 coating, reproduced with permission from [92]. Copyright 2021, Elsevier B.V.; (**e**) the preparation process of M-TiO_2, superhydrophobic M-TiO_2 coating, and M-TiO_2@EP coating; (**f**) the static contact angle for water droplets on the M-TiO_2@EP coating surface under different pH and self-cleaning ability test of M-TiO_2@EP coating with graphite powder as impurity; (**g**) outdoor test sample A (**g**), reproduced with permission from [94]. Copyright 2022, Elsevier B.V.

3.2. Electrodeposition

With the continuous development and diversification of technology, the electrodeposition of metal particles on conductive glass substrate has become a mature technology [95,96]. Compared with other deposition methods, electrodeposition has the advantages of low cost, short reaction time, low temperature, easy control, and environmental friendliness [97,98]. The deposition rate and time can be well controlled to obtain a uniform film with controllable composition. Specifically, a suspension for electrodeposition and a conductive glass substrate (mainly indium-doped tin oxide (ITO) and FTO glass) is prepared first. After that, the conductive glass is used as the working electrode, the Pt wire/foil is a counter electrode, and a standard calomel electrode or Ag/AgCl is used as the reference electrode to start the electrodeposition process at a certain deposition voltage and a specific temperature [99]. The coating is formed and may need annealing (Figure 12).

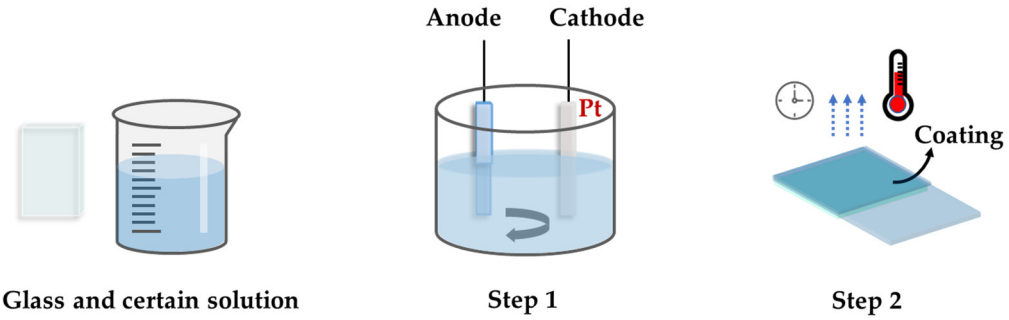


Figure 12. Schematic diagram of the steps in the electrodeposition process (working electrode as anode as an example).

Zhou et al. [100] prepared uniform TiO_2/SiO_2 composite films on ITO glass substrates using electrodeposition. ITO glass served as the cathode and Pt foil served as the anode with a 2 V constant bias. The deposited film was washed with distilled water, and then it was dried and calcined at 450 °C for 2 h. The obtained material was used to evaluate electrochemically assisted photocatalytic degradation of 4-chlorophenol. The photoelectrocatalytic (PEC) activity of the TiO_2/SiO_2 composite film was affected by the deposition time, calcination temperature, and the initial pH value. Furthermore, the electrode potential of PEC experiments was kept at 0.8 V. The results indicated that the PEC activity of the TiO_2/SiO_2 composite film electrode was significantly improved, which was about 14 times higher than that of the pure TiO_2 film electrode. This result was attributed to the incorporation of SiO_2 enhancing the charge separation of photogenerated e^-/h^+ pairs. Moreover, Lu et al. [101] successfully fabricated $TiO_2/CdSe$ heterostructured films using a two-step electrodeposition method for the first time. Firstly, the anatase TiO_2 films were electrodeposited on FTO conductive glass using $TiOSO_4$ as the precursor, and then CdSe was electrodeposited on the obtained TiO_2 glass substrate with $CdCl_2$ and SeO_2 as precursors (Figure 13a). The two-step deposition process was completed under different electrodeposition parameters. The deposition voltages of TiO_2 and CdSe were −1.2 V and −0.5 V, respectively. The heterogeneous structure formation expanded the sunlight absorption range, which led to a more remarkable photocatalytic activity of the $TiO_2/CdSe$ coatings than that of pure TiO_2 single-layer coatings (Figure 13b,c).

Vasile et al. [102] deposited TiO_x thin film from an acidic aqueous solution comprising $TiOSO_4$ on an FTO glass substrate by cathodic electrodeposition at −1.05 V. Then, FTO/TiO_x was used as the anode, and a platinum foil was used as the cathode to deposit FeOOH at 1.2 V. After the deposition, $FTO/TiO_x/FeOOH$ was annealed to obtain $FTO/TiO_2/Fe_2O_3$ structure. TiO_2/Fe_2O_3 had a compact cauliflower morphology with a deposition thickness of about 100 nm (Figure 13d). It could be observed from the optical absorption spectra of the sample that the TiO_2/Fe_2O_3 composite structure improved the light absorption in the ultraviolet and visible regions, as shown in Figure 13e. The formation of heterostructures also promoted the separation and charge carrier transfer in the hematite–titania composite (see Figure 13f). Consequently, $FTO/TiO_2/Fe_2O_3$, a photoanode for solar water oxidation, had good PEC performance.

3.3. Physical Vapor Deposition (PVD)

3.3.1. Magnetron Sputtering

With the rapid progressive applications of photocatalytic TiO_2-based coatings, magnetron sputtering has become an exciting method for preparing high-purity uniform coatings on glass substrates [103,104]. The basic magnetron sputtering process occurs at reduced pressure (typically 0.1 to 0.5 Pa) [105]. As shown in Figure 14, gas atoms are ionized by electric and magnetic fields to produce gas^+ and electrons, which bombard the target (or cathode) with high energy, causing the metal on the target surface to be sputtered in atomic or ionic states and condensed into a thin film on the substrate [106]. Oxygen

or nitrogen as reactive gases can be introduced with inlet gas to form composite films of oxides or nitrides. According to the current mode, magnetron sputtering can be divided into direct current (DC) magnetron sputtering (suitable for conductive targets) and radio frequency (RF) magnetron sputtering (suitable for any target). In addition, magnetron sputtering deposition methods can be classified as single-target and multi-target sputtering depending on the number of targets.

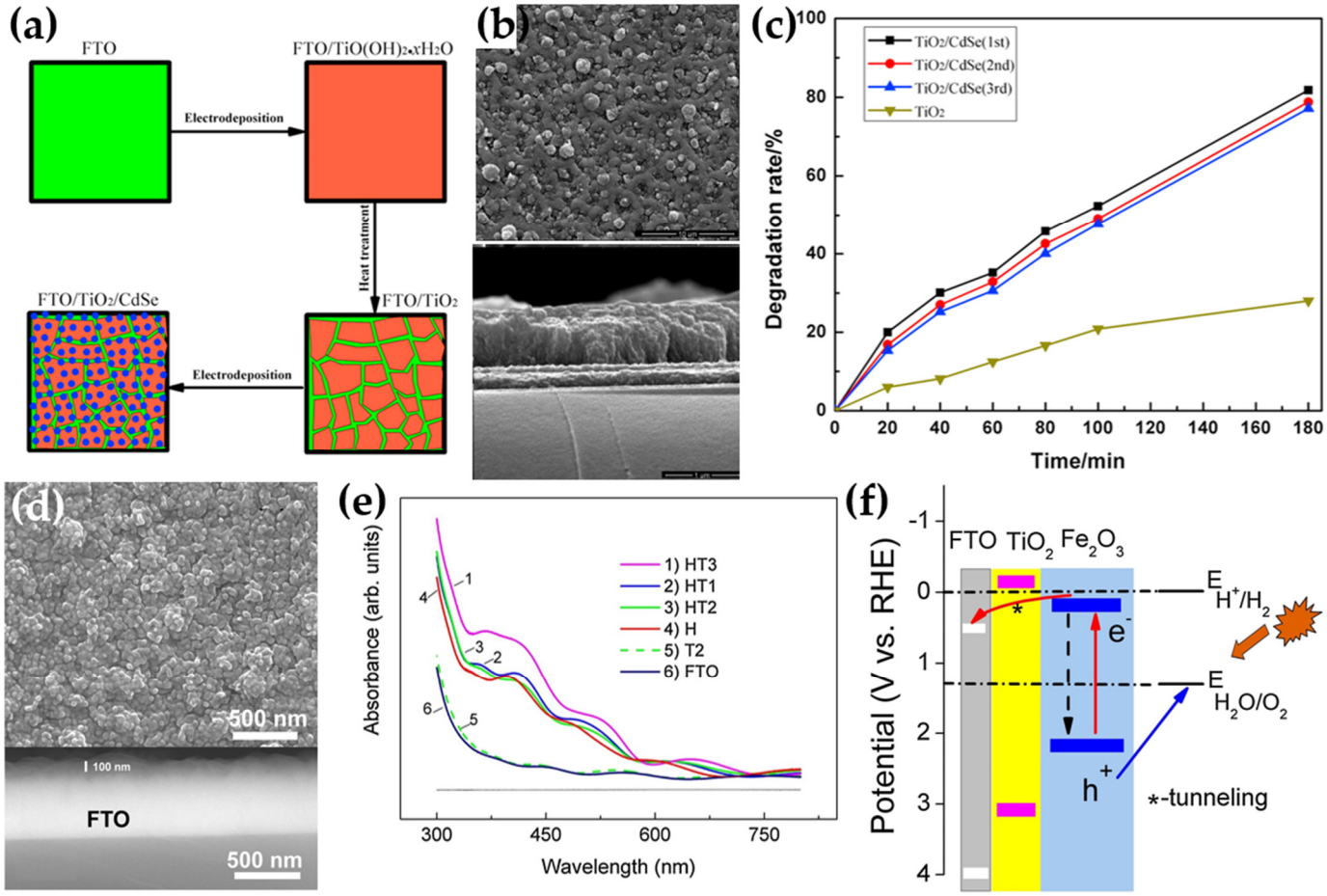


Figure 13. (**a**) Schematic diagram of FTO/TiO_2/CdSe deposition process; (**b**) SEM images of the top-view and the cross-view of TiO_2/CdSe; (**c**) photodegradation rate of MB under illumination, reproduced with permission from [101]. Copyright 2016, Elsevier B.V.; (**d**) FESEM images of the top view and the cross-view of FTO/TiO_2/Fe_2O_3; (**e**) UV-Vis spectra of different samples (HT, H, and T represent FTO/TiO_2/Fe_2O_3, FTO/Fe_2O_3, and FTO/TiO_2, respectively); (**f**) the photocatalytic mechanism of the FTO/TiO_2/Fe_2O_3 photoanodes in PEC water oxidation, reproduced with permission from [102]. Copyright 2019, Elsevier Ltd.

Recently, Mazur et al. [107] deposited TiO_2 and SiO_2 thin films on standard microscope slide glasses, using microwave-assisted reactive magnetron sputtering of high-purity Ti and Si targets. The prepared antireflection multilayer coatings were amorphous, which might be due to the low temperature of the sputtering process (not exceeding 100 °C). Compared with the bare glass substrates, the deposited TiO_2/SiO_2 coated glass had a series of excellent properties, such as antireflectivity, photocatalytic activity, higher hardness, and transmittance. Therefore, the antireflection multilayer coatings could be used as self-cleaning and protective surfaces. Similarly, Villamayor et al. [108] deposited TiO_2 and NiO/TiO_2 coatings using DC and pulsed DC reactive magnetron sputtering on glass slides and monocrystalline silicon wafers as substrates. After deposition, annealing of the coatings at 450 °C for 2 h was performed to obtain anatase TiO_2. The TiO_2 coating had a

columnar porous structure with a thickness of about 740 nm (Figure 15a). The introduction of NiO could change the surface morphology of the TiO_2 coating. NiO/TiO_2 coatings with NiO thicknesses of 10 nm and 20 nm were obtained at sputtering powers of 25 W and 50 W, respectively. When the deposited NiO thickness was increased up to 20 nm from 10 nm, the small cluster-like structure became a cauliflower-like structure, obviously changing surface morphology (see Figure 15b,c). The increased sputtering power made the film more compact and reduced the surface roughness (Figure 15d,e). The formation of a p-n heterojunction also improved the reduction of bandgap value and the mobility of charge carriers, resulting in a higher MB degradation efficiency on NiO/TiO_2 coatings (Figure 15f,g). Interestingly, the test samples had higher photocatalytic efficiency than the commercial Pilkington Activ glass sample. In addition, the results suggested that controlling the deposition thickness and morphology of the NiO layer on TiO_2 films was necessary. The decrease in photocatalytic activity of the thicker coating might be due to the increase in p-n heterojunctions, which counteracts the influence of the decrease in surface area.

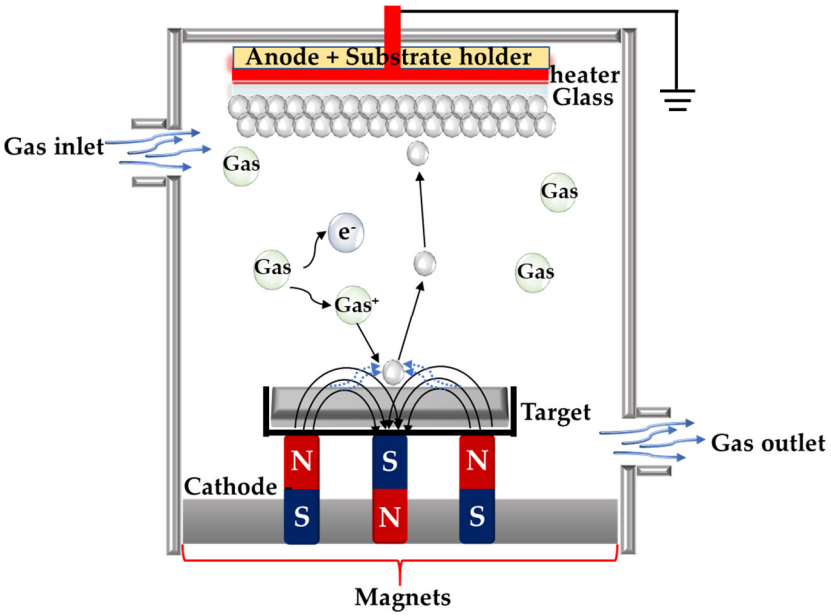


Figure 14. Scheme of the magnetron sputtering process.

Ratova et al. [109] used pulsed DC magnetron sputtering of one target (Ti) in reactive mode for an undoped TiO_2 coating in an Ar/O_2 mixture atmosphere or N-doped TiO_2 coatings in an Ar/dry air atmosphere. It can be observed from Figure 16a that the film deposited in O_2 was uniform with a smooth surface. After the deposition on soda lime glass slides, no additional substrate heating was provided, and the deposition process temperature was below 150 °C. At this time, the study found that the crystallization of the TiO_2 coatings depended on the process pressure, pulse repetition rate, and duty cycle. In addition, although the N-doping led to a narrower band gap, it caused faster recombination of the active photoproduction species. Therefore, N doping did not cause an improvement in photocatalytic activity. The results showed that the TiO_2 coatings had the highest photocatalytic activity for methylene blue and stearic acid (SA) under the conditions of working pressure of 4 Pa, pulse repetition frequency of 100 kHz, and duty cycle of 50% in Ar/O_2 atmosphere (Figure 16b,c). Similarly, Ji et al. [110] combined a thermochromic VO_2 with a photocatalytic TiO_2 layer by reactive DC magnetron sputtering to obtain multifunctional TiO_2/VO_2 bilayer coatings on heated glass. The TiO_2/VO_2 bilayer coating and TiO_2 coating had similar surface morphology, but the TiO_2/VO_2 bilayer film was less smooth than the TiO_2 film due to the presence of VO_2 (Figure 16d,e). Incorporating VO_2 synergistically enhanced thermochromic, luminous, and photocatalytic performances.

As shown in Figure 16f, the bilayer TiO_2/VO_2 coatings lead to glazing that can purify indoor air and lower solar energy inflow, which are essential for energy-efficient buildings with reduced needs for ventilation and air conditioning. The photocatalytic properties of the samples were evaluated based on the SA decomposition reaction. The results showed that the degradation rate of TiO_2/VO_2 bilayer coatings was much faster than that of TiO_2 films under Xenon lamp illumination with or without an AM1.5 filter (Figure 16g,h). The TiO_2/VO_2 bilayer coatings had better performances in terms of light transmittance, indoor air purification, and solar energy modulation.

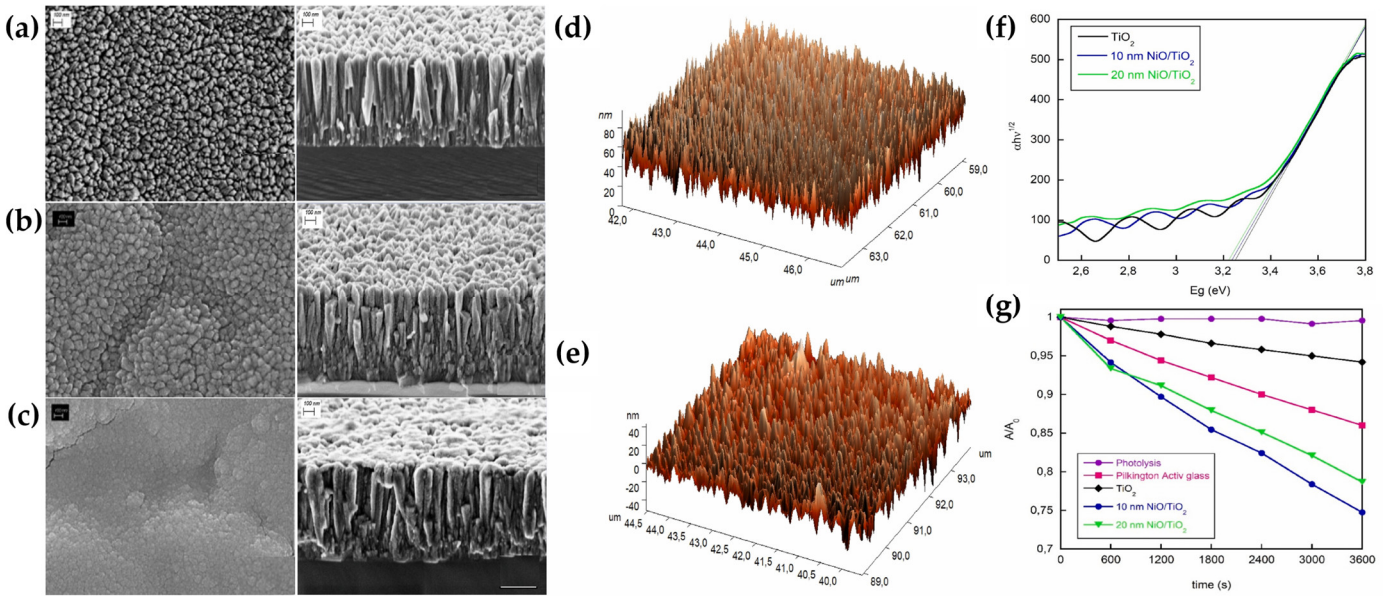


Figure 15. SEM images of (**a**) TiO_2, (**b**) 10 nm NiO/TiO_2, and (**c**) 20 nm NiO/TiO_2 coatings over a silicon substrate; 3D-AFM images of (**d**) 10 nm NiO/TiO_2 and (**e**) 20 nm NiO/TiO_2 coatings; (**f**) optical bandgap of all samples; (**g**) the degradation rate of MB by photocatalytic coatings under UV light, reproduced with permission from [108]. Copyright 2023, Elsevier Ltd. and Techna Group S.r.l.

3.3.2. Pulsed Laser Deposition

Pulsed laser deposition (PLD) is a physical vapor deposition technique. The technique uses high-energy laser pulses to vaporize the target material, generating plasma plumes from the target, and then transporting and condensing atoms onto the glass substrate to obtain a coating with optical properties [111,112]. Such a deposition process is carried out in the presence of a vacuum, reactive gas (GPLD), or liquid (LPLD) [113]. As shown in Figure 17, this technique allows one to tune the porosity and density of TiO_2-layered films by carefully controlling the process parameters. The obtained specific vertically oriented morphologies can facilitate the transport of photogenerated charge carriers and produce effective visible light scattering, making it an excellent method for synthesizing photocatalytic coatings with complex structures and composites [114,115].

Linnik et al. [116] prepared ZrO_2-doped TiO_2 targets with different weight percent concentrations and then used PLD technology to deposit ZrO_2/TiO_2 composite coatings on glass substrates. The increase in ZrO_2 content could narrow the bandgap and enhance the light absorption capability. The coatings of ZrO_2/TiO_2 composite were also obtained by depositing in pure O_2 or mixed N_2:CH_4 atmospheres (5:1 or 9:1) to investigate the effects of active atmospheres on photocatalytic reduction of toxic dichromate (Cr(VI)) ions. The results showed that ZrO_2 (10%)/TiO_2 deposited under N_2:CH_4 (5:1) mixture atmosphere had the highest conversion rate of photo-reduced Cr(VI) ions under UV and visible light irradiation. Interestingly, Olvera-Rodríguez et al. [117] deposited multilayer-type $TiO_2/Au/TiO_2$ thin films on a conductive glass substrate using PLD. The film had

about 212 nm total thickness and consisted of six layers of TiO_2 and five layers of Au alternately (Figure 18a). By coupling with the Au layer, the optical properties of the composite coating were improved mainly from the improved light absorption and reduced recombination rate of photogenerated charges (Figure 18b,c). The $TiO_2/Au/TiO_2$ coating with excellent optical properties was used as a photocatalytic photoanode to degrade paracetamol in electro-oxidation (EO) and PEC, respectively. It was found that the PEC degradation rate of paracetamol was faster under the assistance of UVA light irradiation than that of EO (Figure 18d,e). Also, the added Cl^- from NaCl was oxidized at the photoanode to form active chlorine under UVA light irradiation, which could also degrade paracetamol. Thus, the degradation rate was faster in the presence of Cl^- (Figure 18f).

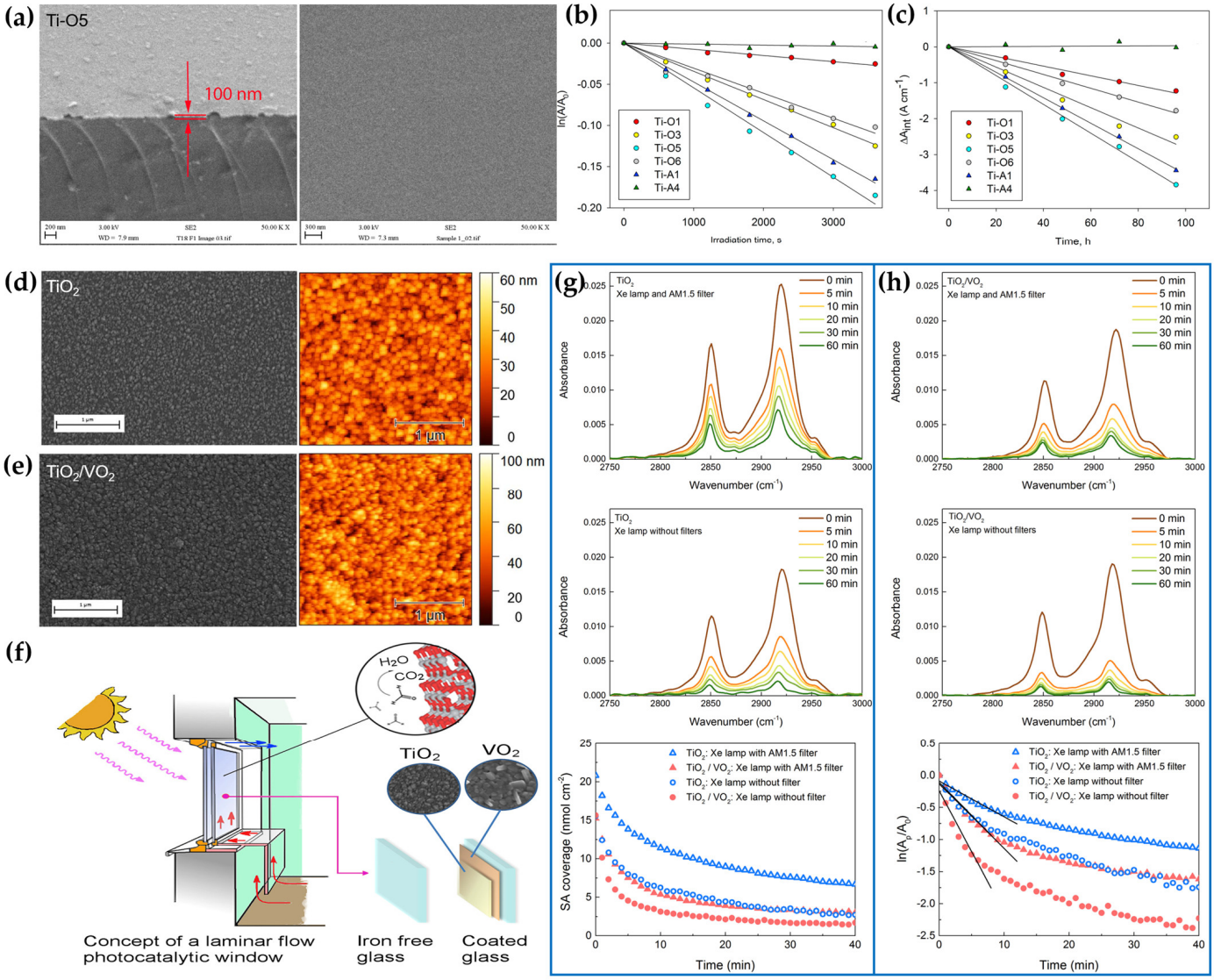


Figure 16. (**a**) SEM cross-sectional view and top view of the Ti-O5 coating; the degradation of (**b**) MB and (**c**) SA by the selected samples under UV light, reproduced with permission from [109]. Copyright 2017, Elsevier Ltd.; surface morphologies of (**d**) TiO_2 and (**e**) TiO_2/VO_2 by SEM (left) and AFM (right); (**f**) scheme of the design principle of a glass window; the degradation of SA under Xenon lamp irradiated with and without AM1.5 filters using (**g**) TiO_2 and (**h**) TiO_2/VO_2, reproduced with permission from [110]. Copyright 2019, Elsevier Inc.

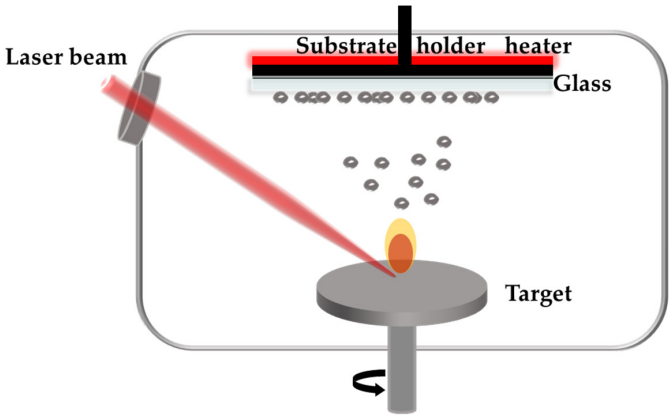


Figure 17. Scheme of the pulsed laser deposition process.

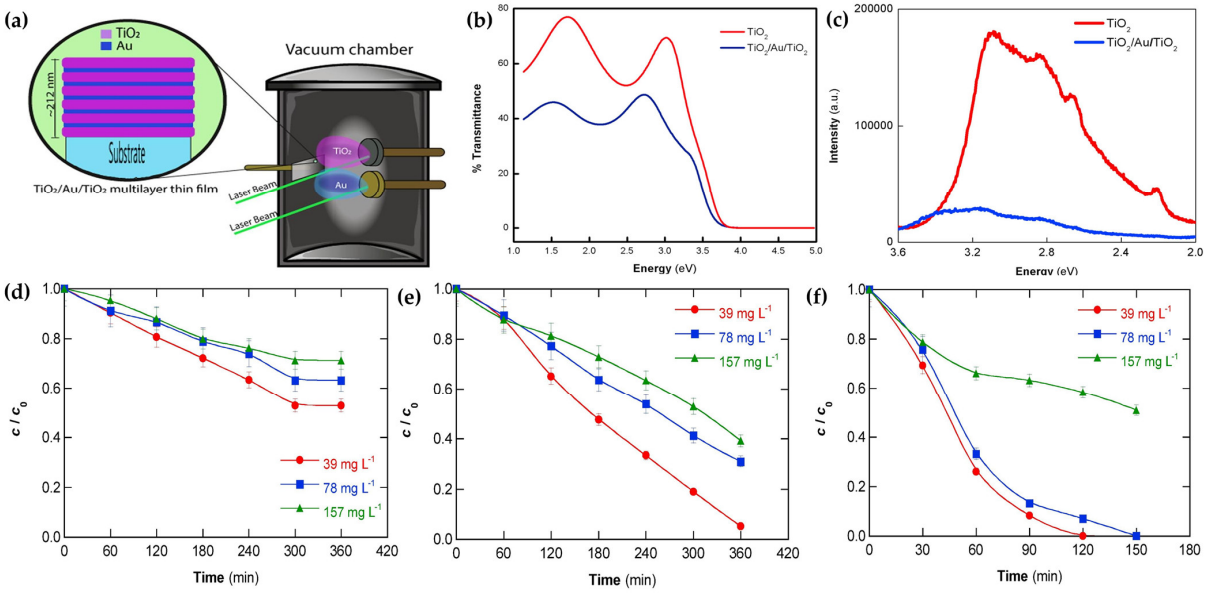


Figure 18. (**a**) Schematic diagram of $TiO_2/Au/TiO_2$ multilayer thin film deposited on glass substrate using PLD; (**b**) the transmission spectra of the TiO_2 thin film and $TiO_2/Au/TiO_2$ multilayer thin film; (**c**) the photoluminescence emission spectrum of the TiO_2 and $TiO_2/Au/TiO_2$ film in the range of 3.6~2.0 eV; the attenuation of paracetamol concentration with electrolysis time using (**d**) EO in 0.050 M Na_2SO_4, (**e**) PEC in 0.050 M Na_2SO_4, and (**f**) PEC in 0.035 M Na_2SO_4 + 0.015 M NaCl, reproduced with permission from [117]. Copyright 2019, Elsevier B.V.

3.4. Chemical Vapor Deposition (CVD)

CVD has unique advantages, such as simple equipment and diverse precursors that allow the fabrication of continuous, compositionally controlled, homogeneous films [118]. Therefore, CVD is a powerful tool for synthesizing high-quality TiO_2-based photocatalytic coatings on various substrate surfaces [119,120]. In a typical CVD process, there are two possible scenarios where the substrate is exposed to volatile precursors. Firstly, the vaporized precursor A reacts with the treated glass substrate and the final product is produced in situ at the glass substrate, or the precursor A is directly deposited on the glass after a chemical reaction (Figure 19a). Alternatively, the vaporized precursor A reacts with the vaporized precursor B, forming thin films on the glass substrate (Figure 19b). Volatile by-products generated during the process are generally removed with the gas stream. Depending on the different precursors, CVD techniques can be defined as aerosol-assisted CVD (AA-CVD), atmospheric pressure CVD (AP-CVD), plasma-enhanced CVD (PE-CVD), or aerosol-assisted metal–organic CVD (AA-MO-CVD).

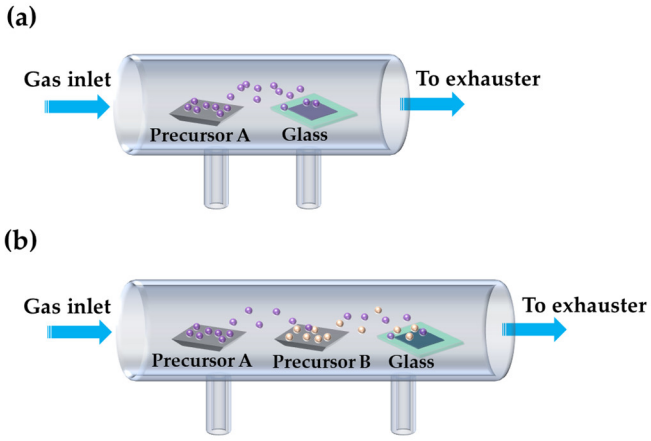


Figure 19. Scheme of the CVD process. (**a**) single precursor, (**b**) multiple precursors.

Alotaibi et al. [121] deposited ZrO_2-TiO_2 composite films on glass substrates by AACVD. The deposition was conducted using zirconium acetylacetonate and titanium isopropoxide as precursors under N_2 atmosphere at 450 °C. After deposition, the glass was cooled down to room temperature in N_2, and then annealed at 600 °C for 1 h. Finally, ZrO_2-TiO_2 composite film showed a dome with cracks, and the thickness of the film was close to 500 nm (Figure 20a,b). Compared with TiO_2 film, ZrO_2-TiO_2 composite film showed better photocatalytic activity in the degradation of resazurin, which was attributed to the improvement of the surface acidity of the composite film (Figure 20c). In addition, there is a high hydroxyl concentration on the surface of ZrO_2-TiO_2 film, which can be used as hole traps to inhibit the recombination of the carrier.

Quesada-González et al. [122] deposited interstitial boron (B)-doped TiO_2 thin films on a float glass substrate using APCVD, starting from boron isopropoxide ($B[(CH_3)_2CHO]_3$) and titanium tetrachloride ($TiCl_4$) as precursors (Figure 20d). The interstitial doping of B caused a change in the morphology of the TiO_2 films, and significantly increased the crystallinity and the average crystallite size. The doping of B did not narrow the band gap, but the recombination rate of e^-/h^+ reduced due to the disordered structure. Thus, the B-TiO_2 films exhibited superior photocatalytic properties for the degradation of SA. Similarly, Sotelo-Vazquez et al. [123] synthesized P-doped TiO_2 thin films deposited on glass by APCVD, using $TiCl_4$ and triethyl phosphate ($(EtO)_3PO$) as precursors. P groups (P^{5+} species and P^{3-} species) affected the photocatalytic activity differently. In the P-TiO_2 composite coatings containing only P^{5+} species, charge carrier concentrations increased by several orders of magnitude, while incorporating P^{3-} species seriously reduced the photogenerated carrier lifetimes. Additionally, the photocatalytic performance of the P ions-TiO_2 composite coatings was also reduced, which was proven in the SA mineralization results.

Lang et al. [124] deposited pristine TiO_2 and Ag NPs-TiO_2 composite films on the quartz glass substrate using PE-CVD, originating from $AgNO_3$ and TTIP as precursors. Then, the obtained coatings were annealed at 600 °C for 12 h to achieve a typical anatase structure under N_2 gas flow at 200 standard cubic centimeters per minute (sccm). The addition of Ag NPs changed the morphology of the films with the appearance of particle aggregation (Figure 20e,f). In addition, doping a moderate amount of Ag NPs could enhance visible light absorption and reduce the bandgap, thus exhibiting significantly higher photocatalytic activity compared with pure TiO_2. However, when excessive Ag NPs were loaded, an e^-/h^+ recombination occurred on the Ag NPs, thus deactivating the carriers and reducing the photocatalytic activity in turn (Figure 20g,h).

Similarly, de Oliveira et al. [125] used AA-MO-CVD to obtain a coating containing TiO_2 and Cu_2O with Ti(IV) oxide bisacetylacetonate and Cu(II) acetylacetonate as precursors at a substrate temperature of 550 °C. The coating was deposited on a (100)-oriented silicon single crystal and alkaline earth boroaluminosilicate glass substrates. The photocatalytic TiCuO composite coatings could be used as a self-cleaning surface to induce an antifouling

activity. The coated glass was immersed in seawater to evaluate its antifouling effect. Marine biofouling field tests proved they had seawater resistant properties and showed a reduced colonization on TiO_2 and 16TiCuO (16 was the atomic percentage of copper measured by EDS) coatings after 38 days (Figure 20i). TiCuO composite coatings are promising, non-toxic fouling release films for marine and industrial applications. However, an effective antifouling surface in practical applications should resist various fouling trophic scales, which requires further research. The photocatalytic experimental results showed that although the optical bandgap decreased with the Cu content increasing, the content of Cu had an optimal value equivalent to that of pure TiO_2 with micro-flowers in degrading Orange G dye (Figure 20j). Under the same experimental conditions, more Cu content was detrimental to the photocatalytic activity (Figure 20k).

3.5. Other Techniques

The advantages and disadvantages of the four deposition techniques in practical applications are shown in Table 1. Each different deposition technique has its own unique characteristics, and even dip coating was able to yield coatings with different properties and applications due to different process parameters. Based on the techniques and applications of TiO_2-based photocatalytic coating deposition on glass substrates mentioned in Section 3, we could couple them to prepare some designed coatings for specific applications. For composite coatings, some research has been carried out using coupling of techniques. Assaker et al. [126] combined spin-coating and electrodeposition techniques to deposit $Znln_2S_4/TiO_2$ composite films on ITO glass. The coupling process is environmentally friendly and avoids high temperatures and pressure. First, the TiO_2 film was deposited on the ITO glass substrate using the spin-coating method. After deposition, the films were dried at 100 °C for 15 min and annealed in O_2 at 450 °C for 1 h. After that, the TiO_2 coating with ITO glass served as the working electrode, and the platinum sheet served as the counter electrode. The nanocrystalline $Znln_2S_4$ films were deposited on the ITO-coated glass substrate using $ZnCl_2$, $InCl_3$, and $Na_2S_2O_3{\cdot}5H_2O$ as the precursors using electrodeposition at room temperature. Due to the homogeneous nucleation process, uniform and dense surface morphology of the three samples was observed (Figure 21a,b), and $Znln_2S_4$ grains with slightly reduced size and round shape were observed on the $Znln_2S_4/TiO_2$ composite film (Figure 21c). TiO_2 had no photocatalytic activity under irradiation of visible light ($\lambda > 420$ nm) due to its wide band gap (3.6 eV). The $Znln_2S_4/TiO_2$ composite coating exhibited higher photocatalytic activity than $Znln_2S_4$ with a narrow bandgap (2.4 eV) (Figure 21d,e). This was mainly due to heterojunction formation between $Znln_2S_4$ and TiO_2, which caused the electron transfer between two conduction bands (Figure 21f). In addition, there are some studies that combine two or more deposition methods to prepare new photocatalytic coatings, and we have not discussed this topic in depth.

Table 1. Advantages and disadvantages of the deposition techniques discussed in Section 3.

Method	Advantages	Disadvantages	Reference
WCD	Simplicity Cost-effectiveness Versatility Larger-scale production	Difficulty in controlling the uniformity of the film layer Low material density and poor adhesion Possible severe cracking Requires post-deposition thermal annealing	[75,83,89]
Electro-deposition	Low cost Environmentally friendly Controllable operation Low-temperature synthesis	Slow dispersion of surface charges and particles in the electrolyte Conductive substrate required Inability to deposit above 80 °C Requires post-deposition thermal annealing	[97,99]

Table 1. *Cont.*

Method	Advantages	Disadvantages	Reference
PVD	Impurity-free High adhesion or durability No harsh chemicals and limited wastes Does not require complex chemical reactions	High temperature and pressure required Often need post-deposition thermal annealing	[108,115]
CVD	Simple equipment Diversified precursor Controllable operation	High temperature (400–900 °C) Disposal and storage of highly corrosive precursors or by-products High cost of high-purity chemicals High toxicity of produced waste gases Often need post-deposition thermal annealing	[119,120]

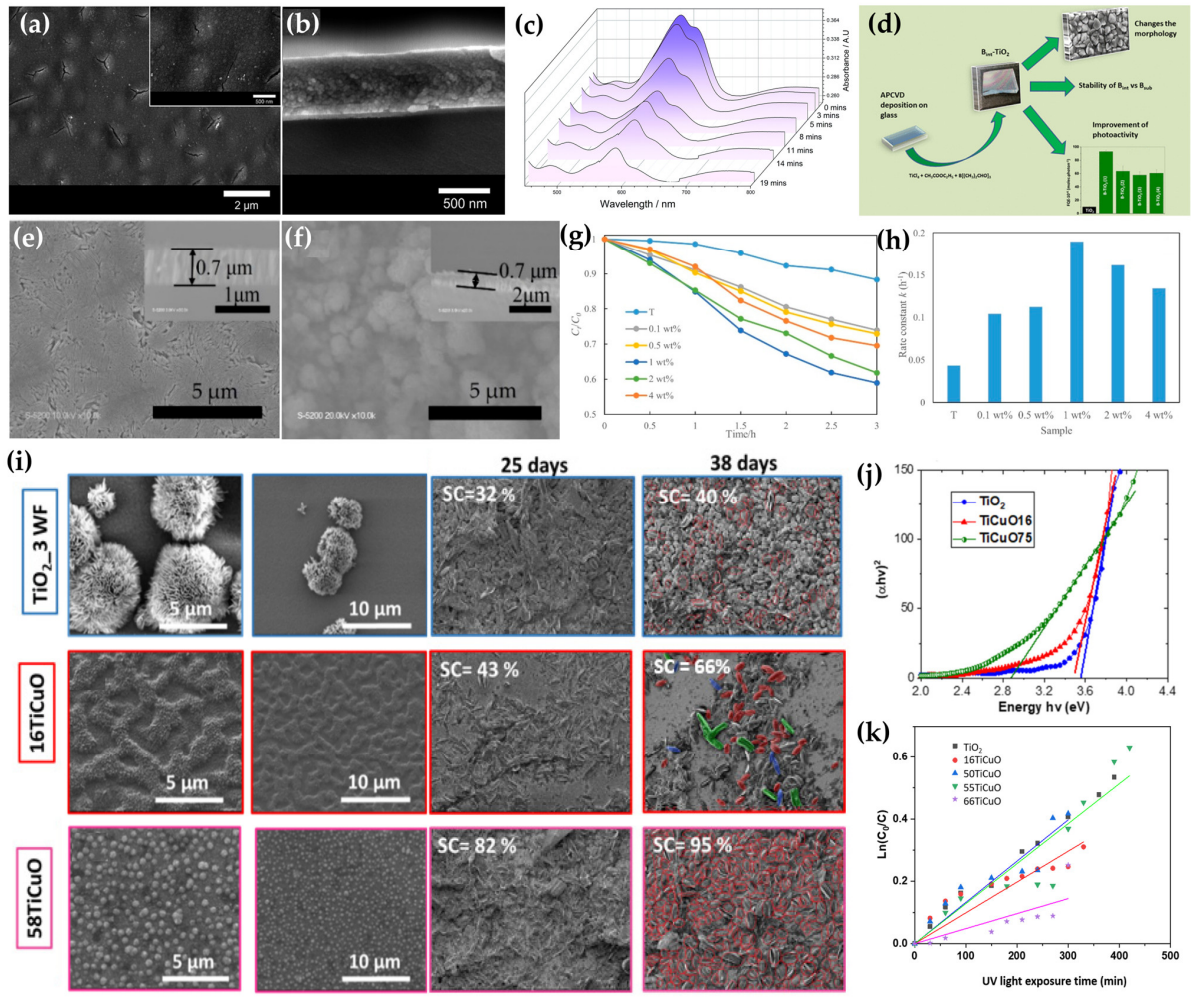


Figure 20. (**a**) SEM top view of ZrO_2-TiO_2 composite films; (**b**) ZrO_2-TiO_2 composite showing the film thickness; (**c**) the degradation of resazurin redox dye on the ZrO_2-TiO_2 composite thin films under UVA irradiation, reproduced with permission from [121]. Copyright 2015, Royal Society of Chemistry; (**d**) scheme of the significant effect of boron on TiO_2 coatings grown by APCVD, reproduced with permission from [122]. Copyright 2016, American Chemical Society; SEM images of the surface and cross-section of (**e**) pristine TiO_2 film and (**f**) Ag (1 wt.%)-TiO_2; (**g**,**h**) the degradation of MB over different films [124]; (**i**) the changes of surface morphology shown by SEM images indicated coatings' colonizations over time of immersion in the Atlantic Ocean for different samples; (**j**) the $(\alpha hv)^{1/2}$ change of the three coatings with energy; (**k**) the degradation kinetics of Orange G by the TiO_2 and various Ti-Cu-O coatings under irradiation of UV (371 nm) [125].

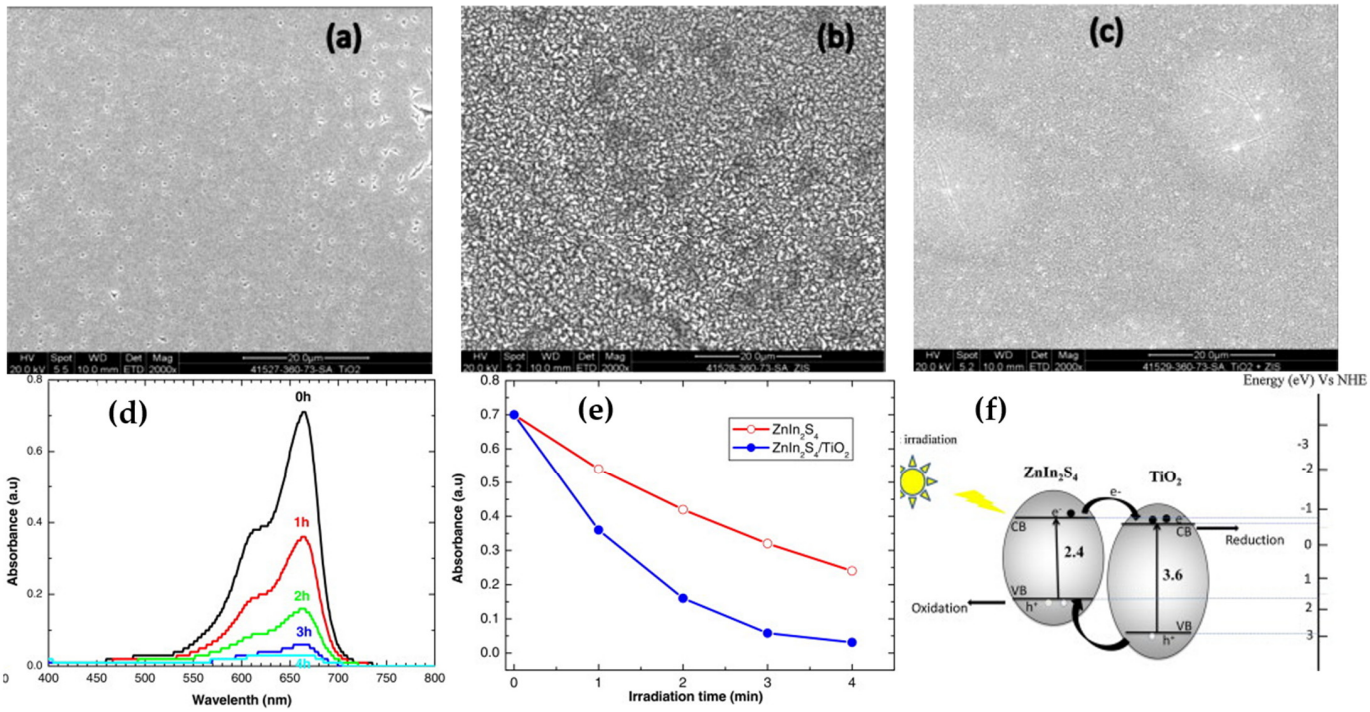


Figure 21. SEM images of (**a**) TiO_2 thin films, (**b**) $ZnInS_4$, and (**c**) $ZnInS_4/TiO_2$; (**d**) the absorption spectra of MB along with time under the irradiation of visible light; (**e**) the photocatalytic removal of MB with $ZnInS_4$ and $ZnInS_4/TiO_2$ under visible light irradiation; (**f**) photocatalytic schematic diagram of $ZnInS_4/TiO_2$ heterojunction, reproduced with permission from [126]. Copyright 2015, Elsevier B.V.

4. Conclusions and Perspectives

In summary, the research progress of TiO_2-based heterogeneous photocatalytic coatings deposited on glass substrates is reviewed in this paper. The photocatalytic properties and applications of the heterogeneous coatings are discussed, from the deposition techniques to photocatalytic applications. The deposition techniques presented in this review involve wet chemical deposition, electrodeposition, physical vapor deposition, and chemical vapor deposition. No ideal method exists, and each technique has specific specifications and characteristics. It is necessary to analyze the final properties and applications of the required photocatalytic coatings and determine the most suitable technology to address specific challenges. Coupling different techniques to develop composite coatings using the advantages of each deposition technique is a good option, but there are few related studies.

There is no denying that TiO_2-based photocatalytic coatings have excellent application potential to overcome the current environmental and energy challenges. Large-scale photocatalytic coatings for practical applications must be durable and sustainable. Therefore, we must fully explore the long-term performance of larger-scale stable TiO_2-based heterogeneous coatings with efficient photocatalytic performances. Coupling different deposition techniques to take advantage of each technique would be a solution for improving photocatalytic deposition performance. Unfortunately, the use of combined methods is often incompatible with industrial processes. At present, it is still the best prospect to improve the photocatalytic performance of TiO_2-based coatings by using the plasma characteristics and metal–semiconductor junction effect of metal NPs. And the incorporation of larger-scale stable TiO_2-based heterogeneous coatings is mainly achieved using the following aspects to improve the photocatalytic properties of TiO_2 coatings: (1) narrowing the bandgap of TiO_2; (2) reducing the recombination rate of e^-/h^+; (3) enhancing the light absorption capacity; and (4) controlling the surface morphology. However, it should be noted that the concentration level of the dopant will affect the improvement of the performance of TiO_2-based

coatings. Excessive doping or loading may result in e^-/h^+ pair recombination, which may cause a decrease in photocatalytic performance. In addition to excellent photocatalytic properties, the composite coating achieves considerable self-cleaning, antireflective, mechanical and antibacterial properties. Therefore, TiO_2-based heterogeneous photocatalytic coatings have a bright future, which could be applied in many applications for practical environmental control.

Author Contributions: Writing—original draft preparation, S.T., Y.F. and Z.Z.; Writing—review and editing, S.T. and Z.H.; Conceptualization, supervision, Z.H. All authors have read and agreed to the published version of the manuscript.

Funding: This research was funded by the Natural Science Foundation of China (No. 22002071 & 22278245), the Young Taishan Scholars Program of Shandong Province (No. tsqn.201909026), and the Shandong University Future Youth Grant Program (No. 61440089964189).

Institutional Review Board Statement: Not applicable.

Informed Consent Statement: Not applicable.

Data Availability Statement: Not applicable.

Conflicts of Interest: The authors declare no conflict of interest.

Abbreviations

TiO_2: Titanium dioxide; WCD, Wet chemical deposition; PVD, Physical vapor deposition; CVD, Chemical vapor deposition; AOPs, Advanced oxidation process; NPs, Nanoparticles; Eg, Bandgap; VB, Valence band; CB, Conduction band; e^-, Photogenerated electron; h^+, Positivity-charged hole; $O_2^{\bullet -}$, Superoxide anion radical; •OH, Hydroxyl radical; •OOH, hydroperoxide radical; BB-41, Basic Blue 41; MB, Methylene blue; ZOC, Zirconium (IV) oxychloride octahydrate; TTIP, Titanium (IV) isopropoxide; RMS, Root mean square; FTO, Fluorine-doped tin oxide; RB 19, reactive blue 19; Au, Gold; SOG, Spin-on-glass; EY, Eosin yellow; EP, Epoxy resin; F-PMHS, Fluorine-containing hydrogen-containing polysiloxane; ITO, Indium-doped tin oxide; PEC, Photoelectrocatalytic; DC, Direct current; RF, Radio frequency; SA, Stearic acid; PLD, Pulsed laser deposition; Cr(VI), Dichromate; EO, Electro-oxidation; AA-CVD, Aerosol-assisted CVD; AP-CVD, Atmospheric pressure CVD; PE-CVD, Plasma-enhanced CVD; AA-MO-CVD, Aerosol-assisted metal-organic CVD; B, Boron; $B[(CH_3)_2CHO]_3$, Boron isopropoxide; $TiCl_4$, Titanium tetrachloride; $(EtO)_3PO$, Triethyl phosphate; sccm, standard cubic centimeters per minute.

References

1. He, Z.; Zhang, J.; Li, X.; Guan, S.; Dai, M.; Wang, S. 1D/2D heterostructured photocatalysts: From design and unique properties to their environmental applications. *Small* **2020**, *16*, 2005051. [CrossRef] [PubMed]
2. van Vliet, M.T.H.; Jones, E.R.; Flörke, M.; Franssen, W.H.P.; Hanasaki, N.; Wada, Y.; Yearsley, J.R. Global water scarcity including surface water quality and expansions of clean water technologies. *Environ. Res. Lett.* **2021**, *16*, 024020. [CrossRef]
3. Dong, F. Two dimensional photocatalytic materials. *Acta Phys.-Chim. Sin.* **2021**, *37*, 2101002. [CrossRef]
4. Zhang, N.; Yang, M.-Q.; Liu, S.; Sun, Y.; Xu, Y.-J. Waltzing with the versatile platform of graphene to synthesize composite photocatalysts. *Chem. Rev.* **2015**, *115*, 10307–10377. [CrossRef] [PubMed]
5. Loeb, S.K.; Alvarez, P.J.J.; Brame, J.A.; Cates, E.L.; Choi, W.; Crittenden, J.; Dionysiou, D.D.; Li, Q.; Li-Puma, G.; Quan, X.; et al. The technology horizon for photocatalytic water treatment: Sunrise or sunset? *Environ. Sci. Technol.* **2019**, *53*, 2937–2947. [CrossRef]
6. Zhang, J.; Dai, M.; Zhang, S.; Dai, M.; Zhang, P.; Wang, S.; He, Z. Recent rrogress on carbon-nanotube-based materials for photocatalytic applications: A review. *Sol. RRL* **2022**, *6*, 2200243. [CrossRef]
7. Xiao, L.H.; Li, X.; Zhang, J.; He, Z.L. MgB_4 MXene-like nanosheets for photocatalytic hydrogen evolution. *ACS Appl. Nano Mater.* **2021**, *4*, 12779–12787. [CrossRef]
8. Zhou, L.; Li, Y.; Zhang, Y.; Qiu, L.; Xing, Y. A 0D/2D $Bi_4V_2O_{11}$/g-C_3N_4 S-scheme heterojunction with rapid interfacial charges migration for photocatalytic antibiotic degradation. *Acta Phys.-Chim. Sin.* **2022**, *38*, 2112027. [CrossRef]
9. Dai, M.; He, Z.; Zhang, P.; Li, X.; Wang, S. $ZnWO_4$-$ZnIn_2S_4$ S-scheme heterojunction for enhanced photocatalytic H_2 evolution. *J. Mater. Sci. Technol.* **2022**, *122*, 231–242. [CrossRef]
10. Sun, T.; Li, C.; Bao, Y.; Fan, J.; Liu, E. S-scheme $MnCo_2S_4$/g-C_3N_4 heterojunction photocatalyst for H_2 production. *Acta Phys.-Chim. Sin.* **2023**, *39*, 2212009. [CrossRef]

11. Dai, M.; Yu, H.; Chen, W.; Qu, K.-A.; Zhai, D.; Liu, C.; Zhao, S.; Wang, S.; He, Z. Boosting photocatalytic activity of $CdLa_2S_4/ZnIn_2S_4$ S-scheme heterojunctions with spatial separation of photoexcited carries. *Chem. Eng. J.* **2023**, *470*, 144240. [CrossRef]
12. Zhang, Y.; Gao, M.; Chen, S.; Wang, H.; Huo, P. Fabricating $Ag/CN/ZnIn_2S_4$ S-scheme heterojunctions with plasmonic effect for enhanced light-driven photocatalytic CO_2 reduction. *Acta Phys.-Chim. Sin.* **2023**, *39*, 2211051. [CrossRef]
13. Cao, W.R.; He, Z.L.; Dai, M.; Wang, G.Z.; Huang, G.H.; Wang, S.G. Electronic structure modulation of bimetallic sulfides for efficient sacrificial-agent-free photocatalytic H_2 evolution. *ACS Appl. Energy Mater.* **2023**, *6*, 4715–4723. [CrossRef]
14. Li, X.; Chang, J.; Zhang, S.; Xiao, L.; Wu, X.; He, Z. Microcystis@TiO_2 nanoparticles for photocatalytic reduction reactions: Nitrogen fixation and hydrogen evolution. *Catalysts* **2021**, *11*, 1443. [CrossRef]
15. Yu, H.; Xu, S.; Zhang, S.; Wang, S.; He, Z. In-Situ construction of core–shell structured TiB_2-TiO_2@g-C_3N_4 for efficient photocatalytic degradation. *Appl. Surf. Sci.* **2022**, *579*, 152201. [CrossRef]
16. Zhang, S.J.; He, Z.L.; Xu, S.S.; Li, X.; Zhang, J.; Zhan, X.P.; Dai, M.; Wang, S.G. In Situ liquid-phase growth strategies of g-C_3N_4 solar-driven heterogeneous catalysts for environmental applications. *Sol. RRL* **2021**, *5*, 2100233. [CrossRef]
17. Toloman, D.; Stefan, M.; Macavei, S.; Barbu-Tudoran, L.; Popa, A. Photocatalytic self-cleaning PVDF membrane blended with MWCNT-ZnO nanocomposites for RhB removal. *Coatings* **2023**, *13*, 594. [CrossRef]
18. Flores-Carrasco, G.; Rodriguez-Pena, M.; Urbieta, A.; Fernandez, P.; Rabanal, M.E. ZnO nanoparticles with controllable Ce content for efficient photocatalytic degradation of MB synthesized by the polyol method. *Catalysts* **2021**, *11*, 71. [CrossRef]
19. Lv, Y.-R.; Liu, C.-J.; He, R.-K.; Li, X.; Xu, Y.-H. $BiVO_4/TiO_2$ heterojunction with enhanced photocatalytic activities and photoelectochemistry performances under visible light illumination. *Mater. Res. Bull.* **2019**, *117*, 35–40. [CrossRef]
20. Liu, X.; Huang, W.-Y.; Zhou, Q.; Chen, X.-R.; Yang, K.; Li, D.; Dionysiou, D.D. Ag-decorated 3D flower-like Bi_2MoO_6/rGO with boosted photocatalytic performance for removal of organic pollutants. *Rare Met.* **2020**, *40*, 1086–1098. [CrossRef]
21. Chen, W.; Dai, M.; Xiang, L.; Zhao, S.; Wang, S.; He, Z. Assembling S-scheme heterojunction between basic bismuth nitrate and bismuth tungstate with promoting charges' separation for accelerated photocatalytic sulfamethazine degradation. *J. Mater. Sci. Technol.* **2023**, in press. [CrossRef]
22. Yu, C.L.; Wei, L.F.; Chen, J.C.; Zhou, W.Q.; Fan, Q.Z.; Yu, J. Novel $AgCl/Ag_2CO_3$ heterostructured photocatalysts with enhanced photocatalytic performance. *Rare Met.* **2016**, *35*, 475–480. [CrossRef]
23. Ping, M.M.; Qiu, S.J.; Wei, G.J.; Liu, J.X.; Wang, Z.J.; Wang, S.T.; An, C.H. Monolith free-standing plasmonic PAN/Ag/AgX (X = Br, I) nanofiber mat as easily recoverable visible-light-driven photocatalyst. *Rare Met.* **2019**, *38*, 361–368. [CrossRef]
24. He, Z.L.; Que, W.X.; He, Y.C. Enhanced photocatalytic performance of sensitized mesoporous TiO_2 nanoparticles by carbon mesostructures. *RSC Adv.* **2014**, *4*, 3332–3339. [CrossRef]
25. He, Z.; Kim, C.; Jeon, T.H.; Choi, W. Hydrogenated heterojunction of boron nitride and titania enables the photocatalytic generation of H_2 in the absence of noble metal catalysts. *Appl. Catal. B Environ.* **2018**, *237*, 772–782. [CrossRef]
26. Zhang, S.; Dai, M.; Guo, J.; Wang, G.; Wang, S.; He, Z. Stable Ti^{3+} in B-TiO_2/BN based hybrids for efficient photocatalytic reduction. *Chem. Eng. J. Adv.* **2022**, *11*, 100333. [CrossRef]
27. Bai, Y.; Xu, S.; Chen, J.; Sun, X.; Zhao, S.; Chang, J.; He, Z. Ti_3C_2@g-C_3N_4/TiO_2 ternary heterogeneous photocatalyst for promoted photocatalytic degradation activities. *Coatings* **2023**, *13*, 655. [CrossRef]
28. Ji, H.; Ni, J.; Zhao, D.; Liu, W. Application of titanate nanotubes for photocatalytic decontamination in water: Challenges and prospects. *ACS EST Eng.* **2022**, *2*, 1015–1038. [CrossRef]
29. Wang, Z.; Xu, S.; Cai, J.; Ma, J.; Zhao, G. Perspective on photoelectrocatalytic removal of refractory organic pollutants in water systems. *ACS EST Eng.* **2022**, *2*, 1001–1014. [CrossRef]
30. Yu, H.; Dai, M.; Zhang, J.; Chen, W.; Jin, Q.; Wang, S.; He, Z. Interface engineering in 2D/2D heterogeneous photocatalysts. *Small* **2023**, *19*, 2205767. [CrossRef]
31. He, Z.; Que, W.; Chen, J.; Yin, X.; He, Y.; Ren, J. Photocatalytic degradation of methyl orange over nitrogen-fluorine codoped TiO_2 nanobelts prepared by solvothermal synthesis. *ACS Appl. Mater. Interfaces* **2012**, *4*, 6816–6826. [CrossRef] [PubMed]
32. Wu, Y.; Li, Y.; Hu, H.; Zeng, G.; Li, C. Recovering hydrogen energy from photocatalytic treatment of pharmaceutical-contaminated water using Co_3O_4 modified {001}/{101}-TiO_2 nanosheets. *ACS EST Eng.* **2021**, *1*, 603–611. [CrossRef]
33. Amoros-Perez, A.; Lillo-Rodenas, M.A.; Roman-Martinez, M.D.; Garcia-Munoz, P.; Keller, N. TiO_2 and TiO_2-carbon hybrid photocatalysts for Diuron removal from water. *Catalysts* **2021**, *11*, 457. [CrossRef]
34. Li, Y.; Zhang, M.Q.; Liu, Y.F.; Zhao, Q.H.; Li, X.; Zhou, Q.Y.; Chen, Y.F.; Wang, S.F. Construction of bronze TiO_2/Ti_3C_2 MXene/Ag_3PO_4 ternary composite photocatalyst toward high photocatalytic performance. *Catalysts* **2022**, *12*, 599. [CrossRef]
35. Wang, L.B.; Fei, X.G.; Zhang, L.Y.; Yu, J.G.; Cheng, B.; Ma, Y.H. Solar fuel generation over nature-inspired recyclable TiO_2/g-C_3N_4 S-scheme hierarchical thin-film photocatalyst. *J. Mater. Sci. Technol.* **2022**, *112*, 1–10. [CrossRef]
36. Zhang, Y.F.; Li, Y.; Yu, H.; Yu, K.; Yu, H.B. Interfacial defective Ti^{3+} on Ti/TiO_2 as visible-light responsive sites with promoted charge transfer and photocatalytic performance. *J. Mater. Sci. Technol.* **2022**, *106*, 139–146. [CrossRef]
37. Weon, S.; Suh, M.J.; Chu, C.; Huang, D.; Stavitski, E.; Kim, J.H. Site-selective loading of single-atom Pt on TiO_2 for photocatalytic oxidation and reductive hydrodefluorination. *ACS EST Eng.* **2021**, *1*, 512–522. [CrossRef]
38. Rosales, A.; Maury-Ramirez, A.; Mejia-De Gutierrez, R.; Guzman, C.; Esquivel, K. SiO_2@TiO_2 coating: Synthesis, physical characterization and photocatalytic evaluation. *Coatings* **2018**, *8*, 120. [CrossRef]

39. Belle, U.; Pelizzari, F.; Lucotti, A.; Castiglioni, C.; Ormellese, M.; Pedeferri, M.; Diamanti, M.V. Immobilized nano-TiO_2 photocatalysts for the degradation of three organic dyes in single and multi-dye solutions. *Coatings* **2020**, *10*, 919. [CrossRef]
40. Qu, K.-A.; Chen, W.; Guo, J.; He, Z. A mini-review on preparation of functional composite fibers and their based devices. *Coatings* **2022**, *12*, 473. [CrossRef]
41. Zhang, J.; Li, X.; Guo, J.; Zhou, G.H.; Xiang, L.; Wang, S.G.; He, Z.L. Novel TiO_2/TPU composite fiber-based smart textiles for photocatalytic applications. *Mater. Adv.* **2022**, *3*, 1518–1526. [CrossRef]
42. Rashid, M.M.; Forte Tavčer, P.; Tomšič, B. Influence of Titanium Dioxide Nanoparticles on Human Health and the Environment. *Nanomaterials* **2021**, *11*, 2354. [CrossRef] [PubMed]
43. Fiordaliso, F.; Bigini, P.; Salmona, M.; Diomede, L. Toxicological impact of titanium dioxide nanoparticles and food-grade titanium dioxide (E171) on human and environmental health. *Environ. Sci. Nano* **2022**, *9*, 1199–1211. [CrossRef]
44. Garlisi, C.; Trepci, E.; Li, X.; Al Sakkaf, R.; Al-Ali, K.; Nogueira, R.P.; Zheng, L.; Azar, E.; Palmisano, G. Multilayer thin film structures for multifunctional glass: Self-cleaning, antireflective and energy-saving properties. *Appl. Energy* **2020**, *264*, 114697. [CrossRef]
45. Ratova, M.; Marcelino, R.B.P.; de Souza, P.P.; Amorim, C.C.; Kelly, P.J. Reactive magnetron sputter deposition of bismuth tungstate coatings for water treatment applications under natural sunlight. *Catalysts* **2017**, *7*, 283. [CrossRef]
46. Liu, Y.; Choi, C.-H. Superhydrophobic sands for the preservation and purification of water. *Coatings* **2021**, *11*, 151. [CrossRef]
47. Dufner, L.; Ott, F.; Otto, N.; Lembcke, T.; Kern, F. Immobilization of TiO_2 photocatalysts for water treatment in geopolymer based coatings. *Catalysts* **2023**, *13*, 898. [CrossRef]
48. Rtimi, S. Indoor light enhanced photocatalytic ultra-thin films on flexible non-heat resistant substrates reducing bacterial infection risks. *Catalysts* **2017**, *7*, 57. [CrossRef]
49. Raditoiu, V.; Raditoiu, A.; Raduly, M.F.; Amariutei, V.; Gifu, I.C.; Anastasescu, M. Photocatalytic behavior of water-based styrene-acrylic coatings containing TiO_2 sensitized with metal-phthalocyanine Tetracarboxylic acids. *Coatings* **2017**, *7*, 229. [CrossRef]
50. Truppi, A.; Luna, M.; Petronella, F.; Falcicchio, A.; Giannini, C.; Comparelli, R.; Mosquera, M.J. Photocatalytic activity of TiO_2/AuNRs-SiO_2 nanocomposites applied to building materials. *Coatings* **2018**, *8*, 296. [CrossRef]
51. Rosales, A.; Escalante, K.E. SiO_2@TiO_2 composite synthesis and its hydrophobic applications: A review. *Catalysts* **2020**, *10*, 171. [CrossRef]
52. Panniello, A.; Curri, M.L.; Diso, D.; Licciulli, A.; Locaputo, V.; Agostiano, A.; Comparelli, R.; Mascolo, G. Nanocrystalline TiO_2 based films onto fibers for photocatalytic degradation of organic dye in aqueous solution. *Appl. Catal. B Environ.* **2012**, *121–122*, 190–197. [CrossRef]
53. Navabpour, P.; Cooke, K.; Sun, H. Photocatalytic properties of doped TiO_2 coatings deposited using reactive magnetron sputtering. *Coatings* **2017**, *7*, 10. [CrossRef]
54. Watte, J.; Van Zele, M.; De Buysser, K.; Van Driessche, I. Recent advances in low-temperature deposition methods of transparent, photocatalytic TiO_2 coatings on polymers. *Coatings* **2018**, *8*, 131. [CrossRef]
55. Ma, J.; Tian, Z.; Li, L.; Lu, Y.; Xu, X.; Hou, J. Loading nano-CuO on TiO_2 nanomeshes towards efficient photodegradation of Methylene Blue. *Catalysts* **2022**, *12*, 383. [CrossRef]
56. Dell'Edera, M.; Lo Porto, C.; De Pasquale, I.; Petronella, F.; Curri, M.L.; Agostiano, A.; Comparelli, R. Photocatalytic TiO_2-based coatings for environmental applications. *Catal. Today* **2021**, *380*, 62–83. [CrossRef]
57. Fujishima, A.; Honda, K. Electrochemical photolysis of water at a semiconductor electrode. *Nature* **1972**, *238*, 37–38. [CrossRef]
58. Wang, S.; Yang, S.; Quispe, E.; Yang, H.; Sanfiorenzo, C.; Rogers, S.W.; Wang, K.; Yang, Y.; Hoffmann, M.R. Removal of antibiotic resistant bacteria and genes by UV-assisted electrochemical oxidation on degenerative TiO_2 nanotube arrays. *ACS EST Eng.* **2021**, *1*, 612–622. [CrossRef]
59. Zhang, J.; Zhou, P.; Liu, J.; Yu, J. New understanding of the difference of photocatalytic activity among anatase, rutile and brookite TiO_2. *Phys. Chem. Chem. Phys.* **2014**, *16*, 20382–20386. [CrossRef]
60. He, Z.; Que, W.; Chen, J.; He, Y.; Wang, G. Surface chemical analysis on the carbon-doped mesoporous TiO_2 photocatalysts after post-thermal treatment: XPS and FTIR characterization. *J. Phys. Chem. Solids* **2013**, *74*, 924–928. [CrossRef]
61. Feng, X.; Guo, H.; Patel, K.; Zhou, H.; Lou, X. High performance, recoverable Fe_3O_4-ZnO nanoparticles for enhanced photocatalytic degradation of phenol. *Chem. Eng. J.* **2014**, *244*, 327–334. [CrossRef]
62. Kim, B.C.; Jeong, E.; Kim, E.; Hong, S.W. Bio-organic–inorganic hybrid photocatalyst, TiO_2 and glucose oxidase composite for enhancing antibacterial performance in aqueous environments. *Appl. Catal. B Environ.* **2019**, *242*, 194–201. [CrossRef]
63. Velázquez-Palenzuela, A.; Ulusoy, B.; Dam-Johansen, K.; Christensen, J.M. Photo-oxidation of nitrite anions in aqueous solution for the benchmarking of nano-TiO_2 photocatalytic coatings. *Prog. Org. Coat.* **2023**, *175*, 107380. [CrossRef]
64. Khatibnezhad, H.; Ambriz-Vargas, F.; Ben Ettouil, F.; Moreau, C. Role of phase content on the photocatalytic performance of TiO_2 coatings deposited by suspension plasma spray. *J. Eur. Ceram. Soc.* **2022**, *42*, 2905–2920. [CrossRef]
65. Si, Y.; Liu, H.; Yu, H.; Jiang, X.; Sun, D. A heterogeneous TiO_2/$SrTiO_3$ coating on titanium alloy with excellent photocatalytic antibacterial, osteogenesis and tribocorrosion properties. *Surf. Coat. Technol.* **2022**, *431*, 128008. [CrossRef]
66. Sansotera, M.; Kheyli, S.G.M.; Baggioli, A.; Bianchi, C.L.; Pedeferri, M.P.; Diamanti, M.V.; Navarrini, W. Absorption and photocatalytic degradation of VOCs by perfluorinated ionomeric coating with TiO_2 nanopowders for air purification. *Chem. Eng. J.* **2019**, *361*, 885–896. [CrossRef]

67. Özcan, M.; Birol, B.; Kaya, F. Investigation of photocatalytic properties of TiO_2 nanoparticle coating on fly ash and red mud based porous ceramic substrate. *Ceram. Int.* **2021**, *47*, 24270–24280. [CrossRef]
68. Zhao, S.; Kim, S.Y.; Saqlain, S.; Cha, B.J.; Seo, H.O.; Kim, Y.D. Photocatalytic NO abatement by cement blocks covered with Fe–TiO_2 and surface hardening agents: Impacts of Fe–TiO_2 contents of coating solutions. *J. Phys. Chem. Solids* **2023**, *174*, 111159. [CrossRef]
69. Liu, S.-H.; Lin, W.-X. A simple method to prepare g-C_3N_4-TiO_2/waste zeolites as visible-light-responsive photocatalytic coatings for degradation of indoor formaldehyde. *J. Hazard. Mater.* **2019**, *368*, 468–476. [CrossRef]
70. Monmaturapoj, N.; Thepsuwan, W.; Mai-Ngam, K.; Ngernpimai, S.; Klinsukhon, W.; Prahsarn, C. Preparation and properties of hydroxyapatite/titania composite for microbial filtration application. *Adv. Appl. Ceram.* **2014**, *113*, 267–274. [CrossRef]
71. Xu, F.; Wang, T.; Chen, H.; Bohling, J.; Maurice, A.M.; Wu, L.; Zhou, S. Preparation of photocatalytic TiO_2-based self-cleaning coatings for painted surface without interlayer. *Prog. Org. Coat.* **2017**, *113*, 15–24. [CrossRef]
72. Behnajady, M.A.; Moghaddam, S.G.; Modirshahla, N.; Shokri, M. Investigation of the effect of heat attachment method parameters at photocatalytic activity of immobilized ZnO nanoparticles on glass plate. *Desalination* **2009**, *249*, 1371–1376. [CrossRef]
73. Joseph, A.; Vijayanandan, A. Review on support materials used for immobilization of nano-photocatalysts for water treatment applications. *Inorganica Chim. Acta* **2023**, *545*, 121284. [CrossRef]
74. Lu, B.-J.; Lin, K.-T.; Kuo, Y.-M.; Tsai, C.-H. Preparation of high-transparency, superhydrophilic visible photo-induced photocatalytic film via a rapid plasma-modification process. *Coatings* **2021**, *11*, 784. [CrossRef]
75. Mittal, T. Self-cleaning smart photocatalytic coatings for water treatment. *Mater. Today Proc.* **2023**, *78*, 891–894. [CrossRef]
76. Najafidoust, A.; Allahyari, S.; Rahemi, N.; Tasbihi, M. Uniform coating of TiO_2 nanoparticles using biotemplates for photocatalytic wastewater treatment. *Ceram. Int.* **2020**, *46*, 4707–4719. [CrossRef]
77. Manna, S.; Adak, D.; Manna, S.; Maity, S.; Jana, S.; Bhattacharya, R.; Medda, S.K. Antireflection cum photocatalytic with superhydrophilic based durable single layer mesoporous TiO_2-ZrO_2 coating surface for efficient solar photovoltaic application. *Sustain. Energy Technol. Assess.* **2023**, *57*, 103236. [CrossRef]
78. Ohya, Y.; Mishina, J.; Matsuda, T.; Ban, T.; Takahashi, Y. Crystallization and microstructure development of sol-gel derived titanium dioxide thin films with single and multiple layers. *J. Am. Ceram. Soc.* **1999**, *82*, 2601–2606. [CrossRef]
79. Rajendran, K.; Senthil Kumar, V.; Anitha Rani, K. Synthesis and characterization of immobilized activated carbon doped TiO_2 thin films. *Optik* **2014**, *125*, 1993–1996. [CrossRef]
80. Rapsomanikis, A.; Apostolopoulou, A.; Stathatos, E.; Lianos, P. Cerium-modified TiO_2 nanocrystalline films for visible light photocatalytic activity. *J. Photochem. Photobiol. A* **2014**, *280*, 46–53. [CrossRef]
81. Bagheri, M.; Farhadian, M.; Vesali-Naseh, M. Performance evaluation of a novel visible-driven CNT/TiO_2/WO_3/CdS heterojunction in photocatalytic fuel cell: Photodegradation of Reactive Blue 19 and electricity production. *Adv. Powder Technol.* **2023**, *34*, 104088. [CrossRef]
82. Mouele, E.S.M.; Ngqoloda, S.; Pescetelli, S.; Di Carlo, A.; Dinu, M.; Vladescu, A.; Parau, A.C.; Agresti, A.; Braic, M.; Arendse, C.J.; et al. Spin coating immobilisation of C-N-TiO_2 co-doped nano catalyst on glass and application for photocatalysis or as electron transporting layer for perovskite solar cells. *Coatings* **2020**, *10*, 1029. [CrossRef]
83. Huong, H.T.; Nhu, T.T.Q.; Nang, H.X.; Tuan, P.A.; Huy, P.T. Super-hydrophilic Ce^{3+}-doped TiO_2-SiO_2 nanocomposite thin films with high optical transmittance by a simple spin-coating method. *Thin Solid Film.* **2023**, *768*, 139730. [CrossRef]
84. Peeters, H.; Keulemans, M.; Nuyts, G.; Vanmeert, F.; Li, C.; Minjauw, M.; Detavernier, C.; Bals, S.; Lenaerts, S.; Verbruggen, S.W. Plasmonic gold-embedded TiO_2 thin films as photocatalytic self-cleaning coatings. *Appl. Catal. B Environ.* **2020**, *267*, 118654. [CrossRef]
85. Komaraiah, D.; Radha, E.; Sivakumar, J.; Ramana Reddy, M.V.; Sayanna, R. Structural, optical properties and photocatalytic activity of Fe^{3+} doped TiO_2 thin films deposited by sol-gel spin coating. *Surf. Interfaces* **2019**, *17*, 100368. [CrossRef]
86. Romero-Morán, A.; Sánchez-Salas, J.L.; Molina-Reyes, J. Influence of selected reactive oxygen species on the photocatalytic activity of TiO_2/SiO_2 composite coatings processed at low temperature. *Appl. Catal. B Environ.* **2021**, *291*, 119685. [CrossRef]
87. Hernandez-Del Castillo, P.C.; Oliva, J.; Robledo-Trujillo, G.; Rodriguez-Gonzalez, V. Enhancing the eosin-yellowish dye degradation in drinking water by using TiO_2 coatings co-doped with Ni and In. *Environ. Sci. Pollut. Res. Int.* **2023**, *30*, 5258–5266. [CrossRef] [PubMed]
88. Wen, K.; Liu, M.; Liu, X.Z.; Deng, C.M.; Zhou, K.S. Deposition of photocatalytic TiO_2 coating by modifying the solidification pathway in plasma spraying. *Coatings* **2017**, *7*, 169. [CrossRef]
89. Suligoj, A.; Pliekhova, O.; Vodisek, N.; Mihelcic, M.; Surca, A.K.; Kunic, R.; Subic, B.; Starman, J.; Ugovsek, A.; Lavrencic Stangar, U. Field test of self-cleaning Zr-modified-TiO_2-SiO_2 films on glass with a demonstration of their anti-fogging effect. *Materials* **2019**, *12*, 2196. [CrossRef]
90. Dundar, I.; Krichevskaya, M.; Katerski, A.; Krunks, M.; Acik, I.O. Photocatalytic degradation of different VOCs in the gas-phase over TiO_2 thin films prepared by ultrasonic spray pyrolysis. *Catalysts* **2019**, *9*, 915. [CrossRef]
91. Zong, L.; Wu, Y.; Li, X.; Jiang, B. The preparation of superhydrophobic photocatalytic fluorosilicone/SiO_2–TiO_2 coating and its self-cleaning performance. *J. Coat. Technol. Res.* **2021**, *18*, 1245–1259. [CrossRef]
92. Wang, X.; Ding, H.; Sun, S.; Zhang, H.; Zhou, R.; Li, Y.; Liang, Y.; Wang, J. Preparation of a temperature-sensitive superhydrophobic self-cleaning SiO_2-TiO_2@PDMS coating with photocatalytic activity. *Surf. Coat. Technol.* **2021**, *408*, 126853. [CrossRef]

93. Wu, B.R.; Lyu, J.J.; Peng, C.Y.; Jiang, D.Z.; Yang, J.; Yang, J.S.; Xing, S.L.; Sheng, L.P. Inverse infusion processed hierarchical structure towards superhydrophobic coatings with ultrahigh mechanical robustness. *Chem. Eng. J.* **2020**, *387*, 124066. [CrossRef]
94. Li, H.; Lai, J.; Yao, M.; Leng, Y.M.; Wu, Z.D.; Zhang, J.; Peng, H.L.; Qiu, Z.M. Development of high performance superhydrophobic coating with excellent corrosion resistance, durability, and self-cleaning properties using M-TiO_2@EP composites. *Appl. Surf. Sci.* **2022**, *601*, 154109. [CrossRef]
95. Gent, E.; Taffa, D.H.; Wark, M. Multi-layered mesoporous TiO_2 thin films: Photoelectrodes with improved activity and stability. *Coatings* **2019**, *9*, 625. [CrossRef]
96. Rosolymou, E.; Spanou, S.; Zanella, C.; Tsoukleris, D.S.; Kohler, S.; Leisner, P.; Pavlatou, E.A. Electrodeposition of photocatalytic Sn-Ni matrix composite coatings embedded with doped TiO_2 particles. *Coatings* **2020**, *10*, 775. [CrossRef]
97. Becker, M.; Yezerska, O. Review—Recent progress in low temperature dynthesis of crystalline TiO_2 photocatalytic films by highly controllable electrodeposition. *J. Electrochem. Soc.* **2022**, *169*, 052507. [CrossRef]
98. Liu, X.; Wang, G.; Zhi, H.; Dong, J.; Hao, J.; Zhang, X.; Wang, J.; Li, D.; Liu, B. Synthesis of the porous ZnO nanosheets and TiO_2/ZnO/FTO composite films by a low-temperature hydrothermal method and their applications in photocatalysis and electrochromism. *Coatings* **2022**, *12*, 695. [CrossRef]
99. Zhang, T.; Wang, T.; Meng, F.; Yang, M.; Kawi, S. Recent advances in $ZnIn_2S_4$-based materials towards photocatalytic purification, solar fuel production and organic transformations. *J. Mater. Chem. C* **2022**, *10*, 5400–5424. [CrossRef]
100. Zhou, Z.X.; Zhu, L.H.; Li, J.; Tang, H.Q. Electrochemical preparation of TiO_2/SiO_2 composite film and its high activity toward the photoelectrocatalytic degradation of methyl orange. *J. Appl. Electrochem.* **2009**, *39*, 1745–1753. [CrossRef]
101. Lu, C.L.; Zhang, L.; Zhang, Y.W.; Liu, S.Y. Electrodeposition of TiO_2/CdSe heterostructure films and photocatalytic degradation of methylene blue. *Mater. Lett.* **2016**, *185*, 342–345. [CrossRef]
102. Vasile, E.; Sima, M.; Sima, A.; Logofatu, C. TiO_2/Fe_2O_3 photoanodes for solar water oxidation prepared via electrodeposition of amorphous precursors. *Mater. Res. Bull.* **2020**, *121*, 110623. [CrossRef]
103. de Oliveira, C.V.; Alhussein, A.; Creus, J.; Schuster, F.; Schlegel, M.L.; Dong, Z.; Jimenez, C.; Sanchette, F. Bifunctional TiO_2/AlZr thin films on steel substrate combining corrosion resistance and photocatalytic properties. *Coatings* **2019**, *9*, 564. [CrossRef]
104. Vahl, A.; Veziroglu, S.; Henkel, B.; Strunskus, T.; Polonskyi, O.; Aktas, O.C.; Faupel, F. Pathways to tailor photocatalytic performance of TiO_2 thin films deposited by reactive magnetron sputtering. *Materials* **2019**, *12*, 2840. [CrossRef]
105. Kelly, P.J.; West, G.T.; Ratova, M.; Fisher, L.; Ostovarpour, S.; Verran, J. Structural formation and photocatalytic activity of magnetron sputtered titania and doped-titania coatings. *Molecules* **2014**, *19*, 16327–16348. [CrossRef]
106. Cui, K.X.; Zhang, Y. High-entropy alloy films. *Coatings* **2023**, *13*, 635. [CrossRef]
107. Mazur, M.; Wojcieszak, D.; Kaczmarek, D.; Domaradzki, J.; Song, S.; Gibson, D.; Placido, F.; Mazur, P.; Kalisz, M.; Poniedzialek, A. Functional photocatalytically active and scratch resistant antireflective coating based on TiO_2 and SiO_2. *Appl. Surf. Sci.* **2016**, *380*, 165–171. [CrossRef]
108. Villamayor, A.; Pomone, T.; Perero, S.; Ferraris, M.; Barrio, V.L.; G-Berasategui, E.; Kelly, P. Development of photocatalytic nanostructured TiO_2 and NiO/TiO_2 coatings by DC magnetron sputtering for photocatalytic applications. *Ceram. Int.* **2023**, *49*, 19309–19317. [CrossRef]
109. Ratova, M.; Klaysri, R.; Praserthdam, P.; Kelly, P.J. Pulsed DC magnetron sputtering deposition of crystalline photocatalytic titania coatings at elevated process pressures. *Mater. Sci. Semicon. Proc.* **2017**, *71*, 188–196. [CrossRef]
110. Ji, Y.; Mattsson, A.; Niklasson, G.A.; Granqvist, C.G.; Österlund, L. Synergistic TiO_2/VO_2 window coating with thermochromism, enhanced luminous transmittance, and photocatalytic activity. *Joule* **2019**, *3*, 2457–2471. [CrossRef]
111. Ding, R.; Wang, K.; Hong, K.; Zhang, Y.; Cui, Y. Hierarchical core-shell tungsten oxide/TiO_2 nanowires as an effective photocatalyst. *Chem. Phys. Lett.* **2019**, *714*, 156–159. [CrossRef]
112. Constantinoiu, I.; Viespe, C. Development of Pd/TiO_2 porous layers by pulsed laser deposition for surface acoustic wave H_2 gas sensor. *Nanomaterials* **2020**, *10*, 760. [CrossRef] [PubMed]
113. Gondal, M.A.; Ilyas, A.M.; Fasasi, T.A.; Dastageer, M.A.; Seddigi, Z.S.; Qahtan, T.F.; Faiz, M.; Khattak, G.D. Synthesis of green TiO_2/ZnO/CdS hybrid nano-catalyst for efficient light harvesting using an elegant pulsed laser ablation in liquids method. *Appl. Surf. Sci.* **2015**, *357*, 2217–2222. [CrossRef]
114. Bricchi, B.R.; Ghidelli, M.; Mascaretti, L.; Zapelli, A.; Russo, V.; Casari, C.S.; Terraneo, G.; Alessandri, I.; Ducati, C.; Li Bassi, A. Integration of plasmonic Au nanoparticles in TiO_2 hierarchical structures in a single-step pulsed laser co-deposition. *Mater. Design.* **2018**, *156*, 311–319. [CrossRef]
115. Kadri, L.; Abderrahmane, A.; Bulai, G.; Carlescu, A.; Doroftei, C.; Motrescu, I.; Gurlui, S.; Leontie, L.; Adnane, M. Optical and structural analysis of TiO_2-SiO_2 nanocomposite thin films fabricated via pulsed laser deposition technique. *Nanomaterials* **2023**, *13*, 1632. [CrossRef]
116. Linnik, O.; Shestopal, N.; Smirnova, N.; Eremenko, A.; Korduban, O.; Kandyba, V.; Kryshchuk, T.; Socol, G.; Stefan, N.; Popescu-Pelin, G.; et al. Correlation between electronic structure and photocatalytic properties of non-metal doped TiO_2/ZrO_2 thin films obtained by pulsed laser deposition method. *Vacuum* **2015**, *114*, 166–171. [CrossRef]
117. Olvera-Rodríguez, I.; Hernández, R.; Medel, A.; Guzmán, C.; Escobar-Alarcón, L.; Brillas, E.; Sirés, I.; Esquivel, K. TiO_2/Au/TiO_2 multilayer thin-film photoanodes synthesized by pulsed laser deposition for photoelectrochemical degradation of organic pollutants. *Sep. Purif. Technol.* **2019**, *224*, 189–198. [CrossRef]

118. Lin, L.; Deng, B.; Sun, J.; Peng, H.; Liu, Z. Bridging the gap between reality and ideal in chemical vapor deposition growth of graphene. *Chem. Rev.* **2018**, *118*, 9281–9343. [CrossRef]
119. Liu, H.Y.; Hsu, Y.-L.; Zheng, Y.X. Investigation of oxygen deficiency-rich/oxygen deficiency-poor stacked TiO_2 based resistive random access memory by mist chemical vapor deposition. *Ceram. Int.* **2022**, *48*, 28881–28888. [CrossRef]
120. Yang, K.; Zhong, S.; Zhou, X.; Tang, S.; Qiao, K.; Ma, K.; Song, L.; Yue, H.; Liang, B. Controllable Al_2O_3 coating makes TiO_2 photocatalysts active under visible light by pulsed chemical vapor deposition. *Chem. Eng. Sci.* **2023**, *277*, 118792. [CrossRef]
121. Alotaibi, A.M.; Sathasivam, S.; Parkin, I.P. Aerosol assisted chemical vapour deposition of a ZrO_2–TiO_2 composite thin film with enhanced photocatalytic activity. *RSC Adv.* **2015**, *5*, 67944–67950. [CrossRef]
122. Quesada-Gonzalez, M.; Boscher, N.D.; Carmalt, C.J.; Parkin, I.P. Interstitial boron-doped TiO_2 thin films: The significant effect of boron on TiO_2 coatings grown by atmospheric pressure chemical vapor deposition. *ACS Appl. Mater. Interfaces* **2016**, *8*, 25024–25029. [CrossRef] [PubMed]
123. Sotelo-Vazquez, C.; Noor, N.; Kafizas, A.; Quesada-Cabrera, R.; Scanlon, D.O.; Taylor, A.; Durrant, J.R.; Parkin, I.P. Multifunctional P-doped TiO_2 films: A new approach to self-cleaning, transparent conducting oxide materials. *Chem. Mater.* **2015**, *27*, 3234–3242. [CrossRef]
124. Lang, J.H.; Takahashi, K.; Kubo, M.; Shimada, M. Ag-doped TiO_2 composite films prepared using aerosol-assisted, plasma-enhanced chemical vapor deposition. *Catalysts* **2022**, *12*, 365. [CrossRef]
125. Villardi de Oliveira, C.; Petitbois, J.; Faÿ, F.; Sanchette, F.; Schuster, F.; Alhussein, A.; Chaix-Pluchery, O.; Deschanvres, J.-L.; Jiménez, C. Marine antibiofouling properties of TiO_2 and Ti-Cu-O films deposited by aerosol-assisted chemical vapor deposition. *Coatings* **2020**, *10*, 779. [CrossRef]
126. Assaker, I.B.; Gannouni, M.; Naceur, J.B.; Almessiere, M.A.; Al-Otaibi, A.L.; Ghrib, T.; Shen, S.; Chtourou, R. Electrodeposited $ZnIn_2S_4$ onto TiO_2 thin films for semiconductor-sensitized photocatalytic and photoelectrochemical applications. *Appl. Surf. Sci.* **2015**, *351*, 927–934. [CrossRef]

Disclaimer/Publisher's Note: The statements, opinions and data contained in all publications are solely those of the individual author(s) and contributor(s) and not of MDPI and/or the editor(s). MDPI and/or the editor(s) disclaim responsibility for any injury to people or property resulting from any ideas, methods, instructions or products referred to in the content.